Neutronic studies in support of accelerator-driven systems: The MUSE experiments in the MASURCA facility

R. Soule, W. Assal, P. Chaussonnet, C. Destouches, C. Domergue, C. Jammes, J.-M. Laurens, J.-F. Lebrat, F. Mellier, G. Perret, et al.

Neutronic Studies in Support of ADS :

The MUSE Experiments in the MASURCA Facility

R. Soule, W. Assal, P. Chaussonnet, C. Destouches, C. Domergue,
C. Jammes, J.-M. Laurens, J.-F. Lebrat, F.Mellier, G. Perret, G. Rimpault, H. Servière

CEA, Centre de Cadarache, F-13108 Saint Paul lez Durance, France

G. Imel

ANL, P.O. Box 2528, Idaho Falls, ID 83403, USA

G.M. Thomas

BNFL, Springfields Works, Preston, Lancashire, England

D. Villamarin, E. Gonzalez-Romero

CIEMAT, Avda. Complutense 22, Madrid, Spain

M. Plaschy, R. Chawla

PSI, CH-5232 Villigen PSI, Switzerland

J.L. Kloosterman, Y.Rugama

IRI, DUT, Mekelweg 15, NL-2629 JB Delft, Netherlands

A. Billebaud*, R. Brissot, D. Heuer, M. Kerveno, C. Le Brun, E. Liatard,
J.-M. Loiseaux, O.Méplan, E. Merle, F. Perdu, J. Vollaire

LPSC(ISN), CNRS-IN2P3/UJF, 53 av. des Martyrs, F-38026 Grenoble Cedex, France

P. Baeten

SCK-CEN, Boeretang 200, 2400 Mol, Belgium

On behalf of the MUSE European Collaboration**

**corresponding author* billebaud@lpsc.in2p3.fr
fax number: +33 4 76 28 40 04

November 1, 2003
Total number of pages: 80
Number of tables: 16
Number of figures: 18

** The MUSE European Collaboration : CEA/DEN Cadarache, ISN Grenoble (France), SCK/CEN Mol (Belgium), BNFL (Great Britain), DUT Delft, NRG Petten (The Netherlands), CIEMAT Madrid (Spain), FZK Karlsruhe, FZJ Jülich (Germany), ENEA Roma (Italy), KTH, CUT (Sweden), UMMET (Poland).

Abstract

The MUSE program (Multiplication with an external source) is in progress at the MASURCA critical facility at the Cadarache Research Center of the CEA in France. The program is dedicated to the physics studies of accelerator driven systems (ADS) in support of transmutation studies of minor actinides and long-lived fission products. It began in 1995 with the coupling of a Cf source in MASURCA, and was followed by a commercial (d,T) source. In 2001, a specially constructed (d,D)/(d,T) neutron generator (GENEPI) was placed in MASURCA, and the MUSE-4 program commenced.

In this paper we describe the first phases of the MUSE-4 program, with data presented that were obtained up to about summer of 2002. We present some results from the 'reference' configuration, which can operate at critical. We present traverses of measured fission reaction rates, with comparison to calculations. Also in the reference configuration we performed activation foil measurements, and also present these results compared to calculations.

Because a major objective of the MUSE program is to test and qualify methods of sub-critical reactivity measurement, we have devoted a major portion of our studies to this area. We have used classical methods (rod-drop, source multiplication) to attempt to measure the subcritical level. In these early phases we studied core configurations of around k_{eff}=0.995. Deeper subcriticality (k_{eff} = 0.96) was achieved by inserting a safety rod.

In addition to the methods mentioned above, we have devoted a lot of effort to pulse neutron source (PNS), fluctuation (Rossi and Feynman-α), and transfer function methods (e.g., CPSD). In this paper we present our preliminary results of all the methods, with some discussion regarding cross-comparison.

I. INTRODUCTION

The commissioning of a future industrial ADS qualified to transmute large amounts of minor actinides and long lived fission products[1] will need numerous technological demonstrations sustained by an extensive basic R&D program in the field of nuclear data, accelerators, spallation targets, fuels and sub-critical systems. As concerns this last theme, the MUSE experiments performed at Cadarache Center (France) in the MASURCA reactor represents a fundamental step for the understanding of the neutronic behaviour of a sub-critical multiplying medium driven by an external neutron source. Conducted in a low power mock-up (power<5kW) where temperature effects are negligible, these experiments are based on the use of a well known external source, in terms of intensity and neutron energy, and they exploit the original idea to separate the experimental validation of the subcritical multiplying medium behaviour from the experimental validation of the source characteristics.

From 1995, the MUSE-1 and then the MUSE-2 experiments, performed with a ^{252}Cf source located at the centre of the MASURCA core, aimed to demonstrate that experimental measurement techniques used for critical cores could be also used for sub-critical configurations. Later, the MUSE-3 experiments constituted the first important parametric study with the loading of several configurations with increasing sub-criticality levels. Based on the use of a commercial neutron generator these experiments helped to optimize the design of the MUSE-4 program and to refine the characteristics of a neutron source, more intense and more suitable to the envisaged measurements. A brief summary of these experiments is given in section II.

Funded by the 5th Euratom Framework Program and supported by the GEDEON French research organizations (newly GEDEPEON), the MUSE-4 experiments are now taking place within the frame of a large international collaboration including sixteen organizations from twelve countries. The three main objectives of this program are:

1- to improve our knowledge of the neutronic behaviour of multiplying media driven by an external neutron source, by experimentally characterising configurations of interest.
2- to define experimental methods allowing the determination of sub-criticality levels (without need to achieve criticality) in support to the operation of an ADS,
3- to define recommended calculation routes for the neutronic predictions of ADS (including nuclear data, calculation tools, biases and residual uncertainties).

The mainspring of the MUSE-4 experiments, the GENEPI (Générateur de Neutrons Pulsés Intenses) neutron generator is born from a close collaboration between CEA and CNRS. Built specifically with a view to these experiments, its main characteristic is to deliver very short pulses (<1μs) with a repetition rate going from a few Hertz to 5 kHz. Details about the setup are given in section III. The measurement program, after a first step of characterization of a critical configuration described in section IV, is based on a parametric approach and the use of many experimental techniques and analysis methods.

Among the neutronic parameters we wish to measure, the determination of reactivity levels is of prime importance. In fact, among the safety demonstrations that will precede the commissioning of an ADS, the proof of the reactivity level mastery will be decisive for the acceptability of such a machine. A large fraction of the efforts of all experimental teams involved in the MUSE program has been devoted to this objective.

In a practical way, two families of analysis methods are used. The first one aims to study the decreasing of the neutron population (prompt or delayed neutrons) after the injection of a neutron source pulse (Pulsed Neutron Source, "PNS" method, section V.A). The second family investigates the neutronic fluctuations in the fission chains (noise measurements, section V.B.).

The first coupling between MASURCA and GENEPI with deuterium target happened the 27th of November 2001. A series of measurements in a slight sub-critical configuration (k_{eff} = 0.994) was performed at the end of year 2001 and the beginning of year 2002 to get not only

preliminary results but, to have also a first feedback on experimental conditions necessary to improve measurements in the next phases. The study of subcritical configurations began again at the beginning of October 2002 to continue until the end of year 2003 with subcriticality levels representative of an industrial ADS (k_{eff} = 0.97 then 0.95).

As concerns the definition of a recommended route for the prediction of ADS features, two main actions have been launched.

First, a calculation benchmark under the auspices of the OECD/NEA has been defined. Sixteen organizations from fourteen countries are taking part in this exercise. Results from the two first of the three steps that compose this benchmark are currently under analysis. Second, the problems related to the propagation and the streaming of the spallation neutrons are investigated in the SAD[a] (Subcritical Assembly in Dubna) experiments. This program aims to study different spallation neutron sources (Pb, Pb-Bi, W targets) produced by the 660 MeV protons of the Dubna synchrotron, with and without the presence of a multiplying medium. These experiments will allow the validation of the transport calculation tools and the nuclear data treating the deep penetration and the activation of the materials far away from the source and the multiplying medium.These two major actions will not be discussed in this paper. In the following all reactivities will be expressed in "pcm" units: one pcm corresponds to a reactivity of 10^{-5}. Moreover for the whole paper and MUSE-4 results, according to a CPSD measurement[2] of β_{eff} giving 335±7 pcm, the β_{eff} value will be settled to 335 pcm (subsequently no error propagation due to this value will be taken into account).

II. REVIEW OF THE MUSE PROGRAMME

II.A. The MUSE-1 and MUSE-2 Experiments

The MUSE-1 and MUSE-2 experiments[3,4] were very short (weeks) experiments performed in 1995 and 1996 to demonstrate the feasibility of neutronic measurements and

[a] International Scientific and Technology Center Project No. 2267

core characterization of a subcritical reactor driven by an external source in MASURCA. In these experiments, a ^{252}Cf source was introduced in the center of the facility, whose reactivity had been lowered to a subcritical level. The reactor was loaded with conventional UO_2-PuO_2 fuel (Pu enrichment ≈ 25%) with sodium coolant.

Core characterization was performed in terms of ^{235}U axial and radial fission rate traverses, and the effect of the axial position of the external source on the flux shape and on the total power level were investigated.

II.B. The MUSE-3 Experiment

The MUSE-3 experiment[5] was performed from February to April 1998 and consisted of introducing a (D,T) 14 MeV neutron generator (SODERN - GENIE26) loaded inside a standard MASURCA subassembly, at the core center of different subcritical configurations, the tritium target being located at the core median plane. The core was cylindrical around the SODERN generator (60 cm high and about 50 cm in diameter) and its composition was MOX fuel with Na as coolant. The reflector was made of Na and Stainless Steel. The GENIE-26 generator produced 150 keV deuteron pulses of a few μs (with a repetition rate of 200 Hz) on a tritium target, providing a source of about 10^8 n/s.

A critical reference was followed by three subcritical configurations of about -500, -1000 and -1500 pcm respectively, which were obtained by unloading peripheral MASURCA subassemblies from the critical reference. In a later phase, the neutron generator was surrounded successively by sodium and pure lead buffers, to modify the importance of the 14 MeV neutrons emitted by the generator. In these two configurations, a subcriticality level of about -5500 pcm was obtained by adjusting the external fuel loading.

A full core characterization was performed in terms of ^{235}U axial and radial fission rate traverses, and the effect of the buffer surrounding the source on the flux shape and on the total power level were investigated[5]. In each subcritical configuration, measurements were also

performed with the generator working in the pulsed mode in order to test a method of reactivity determination using the PNS technique. An example of these measurements is shown in Fig. 1 for several subcritical levels.

Interesting conclusions could be drawn concerning the dependence of the slope of the count rate with reactivity. However the in-depth analysis of these measurements was made very difficult by experimental biases. Indeed it was observed that light materials - used for high voltage insulation inside the generator – thermalized some neutrons in the reactor and perturbed the PNS measurements[6-8]. Because of these problems, only a few of these measurements were analyzed in a satisfactory manner.

Nevertheless, very interesting conclusions could be drawn from this experiment to optimize the design of the MUSE-4 experiment. For example, important recommendations were given to define a new pulsed source and to ameliorate the quality of the experiments and their analysis, such as:

- there should be no light materials in the part of neutron source (GENEPI) in the reactor,
- the monitoring of the external neutron production is essential,
- the detectors and analyzers should have time constants and performances suited for PNS measurements.

In spite of the problems the MUSE-3 experiment was a very fruitful and important step in the MUSE program.

III. EXPERIMENTAL SETUP

III.A. The MASURCA Facility

The MASURCA facility is dedicated to the neutronic studies of fast reactors lattices. The materials of the core are contained in rodlets, along with square platelets. These rodlets or

platelets are put into wrapper tubes having a square section (4 inches) and about 3 meters in height.

These tubes are hung vertically from a horizontal plate supported by a structure of concrete. The core itself can reach 6 000 litres. To build such cores the tubes are introduced from the bottom in order to avoid that the fall of a tube corresponds to a positive reactivity step. The reactivity control is fulfilled by absorber rods in varying number depending on core types and sizes. The control rods are composed of fuel material in their lower part, so that the homogeneity of the core is kept when the rods are withdrawn. The core is cooled by air and is surrounded by a biological shielding in heavy concrete allowing operation up to a flux level of 10^9 n/cm^2.s. Core and biological shielding are maintained at a reduced pressure, relative to the outside environment. The maximum operating power of the facility is limited to 5kWth. Figure 2 presents a picture of a MASURCA core loading from the bottom.

III.B. The Pulsed Neutron Source GENEPI

The GENEPI (GEnérateur de NEutrons Pulsé Intense) accelerator (see Fig. 3) was especially designed and built by ISN Grenoble for the MUSE experiments in the MASURCA facility for brief neutron injections with a very fast intensity decrease (about 500 ns). To do this, deuteron impulses are created, focalized, accelerated and guided onto a deuterium or tritium titanium target (TiD or TiT respectively). The beam peak intensity is about 50 mA with a width of less than 1µs. The repetition rate can vary from a few Hz up to 5 kHz, providing about 3.10^4 neutrons per pulse with the TiD target (~$1.2\text{x}10^8$ n/s at 4 kHz) and about 3.10^6 neutrons per pulse with the TiT target (~$1.2\text{x}10^{10}$ n/s at 4 kHz). The main characteristics of the ion beam are indicated in Table I.

The online monitoring of the neutron production for both deuterium and tritium targets is based on the detection by Si detectors placed upstream of the target of :

- the recoil protons induced by the D(d,p)T reaction which occurs about as often as the D(d,n) ^{3}He reaction on the deuterium target,
- the recoil alpha particles produced by the T(d,n)^{4}He reactions on the tritium target.

The characterization of the neutron production yield is based on the activation analysis of ^{58}Ni foils. For the 2.67 MeV neutrons produced by the D(d,n)^{3}He reactions, the ^{58}Ni(n,p)^{58}Co reaction is used. The 14 MeV neutron spectrum produced by the T(d,n)^{4}He reactions is determined by both the ^{58}Ni(n,2n)^{57}Ni and ^{58}Ni(n,np)^{57}Co reactions induced by neutrons with an energy higher than 13 MeV.

III.C. Core Experimental Configurations

All the MUSE-4 configurations are based on fuel cells composed of equal amounts of fuel and Na representative of a fast Pu burner core (Pu enrichment of ~ 25% with ~ 18% content of ^{240}Pu) with sodium coolant.

The fuel zone is radially and axially reflected by a stainless steel/sodium (75%/25%) shielding. The GENEPI deuteron guide is horizontally introduced at the core mid-plane and the deuterium or tritium target is located at the core centre. To compensate the spatial effect due to the presence of the GENEPI guide in the north part of the loading, the south symmetrical part is loaded with pure lead (99.99% of Pb) simulating the Pb circulation of the target. To simulate the physical presence of a Pb spallation source, a pure square (10 cm thick) lead zone is placed around the GENEPI target.

The reactivity control is fulfilled by four safety rods (SR) composed of B_4C in their upper part and of fuel material in their lower part. In this way, the homogeneity of the core is kept

when all the rods are withdrawn. Moreover, a fine-tuning rod, the pilot rod (PR), allows the achievement of criticality and the expected power level by adjusting its axial position.

As the measurements are based on a parametric approach, mainly four different experimental configurations will be studied :

- a critical one (called Reference), shown in Fig. 4,
- three successive subcritical configurations named SC0, SC2 SC3; k_{eff} being successively of about 0.994, 0.97 and 0.95 respectively: these three configurations will be obtained by replacing radially some peripheral fuel cells by stainless steel/sodium cells.

Several complementary configurations will be obtained from the previous ones by insertion of safety/pilot rods. These asymmetrical configurations will be of interest in the frame of studying the spatial decoupling effects and the excitation of the high order flux harmonics (the flux tilting could be amplified by the external source).

Here are described the first experiments performed in the Reference and SC0 configurations with the $D(d,n)^3He$ source only. The table II resumes the different configurations obtained with the safety and pilot rods for which measurements were performed. It gives also the corresponding value of ρ (in pcm) when it was possible to get it from Source Multiplication method (SM), Modified Source Multiplication method (MSM), MSM factor value correcting the SM value for subcriticalities lower than 1000 pcm, or Rod Drop (RD) measurements. The number of fuel cells for the Reference configuration varies from 1114 to 1115 as it was necessary to compensate the Pu decay between two distant measurement periods.

III.D. Detectors and Measurement Locations

The detectors used for the measurements described in this paper are mainly fission chambers (FC). They are summarized in Table III.

The locations of measurements are summarized in Table IV and shown in Fig. 4. The (X,Y) coordinates give the location of the vertical channel, according to the Fig. 4, and Z gives the coordinate on the vertical axis (X=0, Y=0) centered on the mid-plane of the core. Two radial channels also shown in Fig. 4 allow measurements in the (X,Y) plane: the West-East (W-E) channel (Y=2.1 cm, Z=-9.5 cm), and the South-North (S-N) channel(X=-7.4 cm, Z=-0.6 cm).

For each type of measurement the locations of the detectors used will be specified in the corresponding section.

IV. CHARACTERIZATION OF A CRITICAL CORE: THE REFERENCE CONFIGURATION

IV.A. The Need for the Reference Configuration

The particular problems associated with the characterization of a hybrid driven system are linked to the precise determination of the level of subcriticality, the effective prediction of the importance of the external source and the accurate estimation of the spectral fluctuations due to the heterogeneous central zones (lead, accelerator). In this context, the establishment of a critical configuration, prior to subsequent driven subcritical cores, offers the advantage of system calibration in terms of reactivity. More precisely, rod drop measurements, as presented in section IV.D, yield the reactivity worth of the control and safety rods leading to improved determination of the level of each future subcriticality. This last point is essential to the study of the validity of different dynamics measurements envisaged for the assessment of the level of subcriticality in a future ADS. Moreover, the analysis of the reference configuration facilitates a decoupling of the spectral variations due to the fundamental mode flux distribution (cf. section IV.B.) and the presence of the external source (cf. section IV.C). Therefore, the two following sections quantify the codes' predictive capabilities regarding the spectral perturbations related to the various geometrical interfaces.

IV.B. Spatial Distributions (Traverses)

The work described was carried out in order to support, and ensure the quality of, the MUSE-4 experimental program and to assist with the specification of the core configurations. A range of parameters were generated using a dataset (with a simplified core geometry and set of isotopes) made available to all MUSE-4 partners. This paper will focus on the calculated and measured reaction rate traverses since these are independent from any pre-calculated parameters.

IV.B.1. Calculation Procedure

All of the calculated data reported in this section were generated using the ERANOS[7] deterministic code suite (**E**uropean **R**eactor **AN**alysis **O**ptimised **S**ystem), which was developed by the CEA in collaboration with other R&D organisations. The JEF 2.2 nuclear data library was used throughout this work. Three-dimensional (TGV-VARIANT[9]) neutronic models of the MUSE-4 cores were constructed using the P1 approximation for the anisotropy treatment of the cross-sections and the simplified P3 approximation for the flux (in 33 energy groups). The resultant flux solutions and group constants were then processed using the diverse range of functions embedded within the overall ERANOS calculation scheme.

IV.B.2. Comparison of Calculated and Measured Traverses

A matrix of radial and axial traverses was generated for Reference loading in critical configuration (1115 cells, and ρ=0) in order to compare the predicted and experimental reaction rates. The intention was to confirm that the ERANOS reaction rate predictions are consistent with the measured experimental values. If this is the case, then the total fission rate (and therefore the core power) as calculated by TGV can be accepted with a certain confidence level.

Comparisons are presented in Fig. 5 and 6 between the measured and predicted reaction rates for an axial (L10) and the W-E radial channel with a thermal and a threshold reaction rate.

Note that Figs. 5 to 6 incorporate data for both thermal (^{235}U and ^{10}B) and threshold (^{240}Pu and ^{237}Np) reactions. The axial and radial channels' coordinates are the same as in the previous paragraph. Good agreement is obtained between the measured and predicted reaction rate distributions in the central lead and fissile zones. A similar comparison in the reflector region at thermal energies (see graph 6(a)) shows that some refinements to the ERANOS model or methodology could be required in order to achieve the same degree of accuracy as that attained in the fissile region.

Reaction rate measurements from a subcritical core with GENEPI activated are expected shortly which will hopefully enable the validation matrix for ERANOS to be extended further to subcritical source-driven systems.

IV.C. Spectral Indices Given by Foil Activations

The results of foil activation measurements performed in the Reference critical configuration (1115 cells) are presented in the current section. Comparisons are made with calculations using MCNP-4C[10] to interpret the experimental results and to investigate the capabilities of the stochastic code to reproduce the spectral perturbations in terms of reaction rate variations across the regions of interest, principally near the accelerator/lead, lead/fuel and fuel/reflector interfaces, where spectral fluctuations are more important.

IV.C.1. Experimental Procedures

The choice of foils has been guided mainly by the need to cover as wide a range of threshold energy values as possible. The list of the activation foils employed includes a large number of threshold and non-threshold reactions. Most of the foils are disc-shaped with a

thickness of 0.25mm and a diameter of 9mm. However, for instance, each of the NpO_2 samples used consists of 9 spheres of 0.8mm diameter contained in a titanium box. All activation samples were located inside experimental aluminium rods, which have a cross section of 10mm x 10mm. These rods were inserted into two radial channels (W-E and S-N) and the L11 axial channel. On the basis of calculations, 10 different locations were selected for activation foil irradiations. These locations are indicated in Table V.

Location F1 was considered as a normalization point in an unperturbed region near a calibrated fission chamber. Location F2 permits a study of the impact of the lead region, while F3 and F4 were selected for highlighting the potential core asymmetry. Location F5 characterized lead moderation/multiplication effects, while location F6 provides a useful test of code capabilities to treat streaming effects along the voided accelerator-tube region. Finally, locations F7, F8, F9 and F10 permit a study of spectral variations along the W-E axis. The achievement of accurate foil activation measurements requires particular attention being given to the application of necessary corrections and the treatment of experimental uncertainties. The corrections applied result from either the irradiation conditions (power normalisation, self-shielding, etc.) or from physical effects associated with the γ-counting of the irradiated foils (detector efficiency, γ-self-absorption, coincidence effects, etc...)[11]. Finally, the corrected measured saturated activities are used to deduce results which can be compared with the calculated integral reaction rates.

IV.C.2. Experimental Results and Comparisons with Calculations

The current MCNP-4C analysis of the experiments has been carried out using the JEF-2.2 library[12] for the transport of neutrons in conjunction with the ENDF/B6 dosimetry data files for the calculation of the threshold reaction rates. This calculation scheme has been compared to others via an international benchmarking exercise[13].

The three different non-threshold reactions which have been considered here are captures in ^{115}In, ^{59}Co and ^{64}Zn. Calculation/experiment (C/E) values for the ratios of saturated activities at F2-F6, relative to F1 in each case, are presented in Table VI. The results appear very satisfactory when one considers the corresponding uncertainties. Table VI gives also the MCNP-based C/E values for the threshold reactions. As mentioned earlier, the ENDF/B6 dosimetry file was used in conjunction with MCNP-4C, although it is the JEF-2.2 library which has been employed for the neutron transport calculation. Although generally satisfactory agreement is obtained for F4-F6, significant discrepancies are indicated for F2 and F3, i.e. the prediction of spectral variations in and around the central lead region at high neutron energies appears to be problematic. Further investigations are clearly needed, of both calculation and experimental aspects, to understand these differences.

The spatial variations of two other threshold reactions (^{232}Th and ^{237}Np fission) have been studied, this time in terms of traverses along the W-E axis, i.e. with measurements at locations F7, F8, F9 and F10. For instance, the moderation effects in the central lead region are clearly reflected in the observed decrease of the threshold fission rates (the measured ratio F9/F10 is 0.86 ± 0.05 and 0.94 ± 0.04 for ^{232}Th and ^{237}Np fission, respectively).

In contrast to Table VI, which does not provide a direct indication of the neutron spectrum at the different locations, in Table VII we present calculated and experimental spatial variations of several spectral indices. These have been considered in terms of reaction rate ratios, relative to ^{115}In(n,n'), at locations F2-F3, with the relatively unperturbed core position F1 serving as reference for each index. The reaction ^{115}In(n,n') has been chosen as denominator for the indices, partly because of the high experimental accuracy achieved for its determination and partly because its threshold of 1.2 MeV is relatively low.

The moderation effect of the central lead zone is clearly indicated by the F2/F1 ratios of the spectral indices, the value for the non-threshold reaction rate ^{64}Zn(n,γ) being greater

than 1.0 and those for the higher-threshold reactions being all less than 1.0. Furthermore, the manner in which the effects of the lead region diminish with distance is well quantified by the changes in the spectral indices between F2/F1, F3/F1, F5/F1 and F6/F1. As regards the core asymmetry created by the presence of the accelerator tube and lead zone, this is characterised by the ratios F3/F1 and F4/F1. It is seen that the differences are largely well within the indicated 1-sigma uncertainties, confirming that asymmetry effects are minor when the accelerator is not operating. The corresponding differences in the source-driven subcritical configurations are, of course, expected to be much greater.

As regards the comparison of calculation and experimental results in Table VII, agreement is seen to be well within the indicated uncertainties in most cases. The need is clearly indicated, however, for improving the statistical accuracy of some of the MCNP results.

The present investigations have clearly demonstrated the value of foil activation measurements in the MUSE-4 programme. Use of the currently reported spectral indices for unfolding the neutron spectrum at specific locations is expected to provide useful supplementary information. Similar studies in the subcritical configurations will contribute to the experimental characterisation of other ADS-specific features, e.g. those related to the external source, which have already been investigated numerically[14].

IV.D. Rod Drop Measurements

The inverse point-kinetics method is a well-known method to determine the reactivity worth of the control rods in nuclear reactors. It is based on measuring the power of the reactor by neutron counters and solving the point-kinetics equations to calculate the dynamic reactivity $\rho(t)$[15]:

$$\rho(t) = \beta + \Lambda \frac{d}{dt}\left[\ln n(t)\right] - \lambda\beta \int_{-\infty}^{t} \frac{n(t')}{n(t)} \exp\left[-\lambda(t-t')\right] dt' - \Lambda \frac{s(t)}{n(t)} \qquad (1)$$

Here, β and λ are the delayed neutron fraction and the corresponding precursor decay constant, and Λ is the generation time. Often the source strength $s(t)$ is not known, although methods exist to determine the source strength from measurement[16]. For fast reactors with a very short generation time Λ, the above expression can be simplified using 'micro kinetics'[17]. The result for the reactivity in dollars $\tilde{\rho}(t) = \rho(t)/\beta$ reads[18]:

$$\tilde{\rho}(t) = \frac{1}{n(t)}\left[n(t) + n_0\left(\tilde{\rho}_0 - \exp\left[-\lambda t\right]\right) - \lambda \int_0^t n(t')\exp\left[-\lambda\left(t-t'\right)\right]dt' \right]. \qquad (2)$$

Compared with Eq. (1) this expression has two advantages. First, it does not require the external source strength to be known (although the value of the initial reactivity $\tilde{\rho}_0$ might seems as hard to get as s_0), and secondly it makes no use of the generation time. The latter is a consequence of the fact that use is made of prompt fission chains, instead of individual fissions, which is only valid if the reactivity does not change during a prompt fission chain. For fast reactors, and certainly for MASURCA, this limitation poses no problem. As stated above, a prompt fission chain takes less than 1 μs, while a safety rod drop that reduces the reactivity with about 10$ takes more than one second. This means that the reactivity changes about 0.001$ during a prompt fission chain, which indeed is negligible. For a sub-critical reactor, the duration of a fission chain is even shorter. For six delayed neutron groups, Eq. (2) reads[18]:

$$\tilde{\rho}(t) = \frac{1}{n(t)}\left[n(t) + n_0\left(\tilde{\rho}_0 - \sum_{j=1}^{6}\frac{\beta_j}{\beta}\exp\left[-\lambda_j t\right] \right) - \sum_{j=1}^{6}\lambda_j \frac{\beta_j}{\beta}\int_0^t n(t')\exp\left[-\lambda_j\left(t-t'\right)\right]dt' \right]. \qquad (3)$$

Measurements have been performed starting with the reactor in critical state (Reference 1114 cells). In all experiments, first the fine-tuning rod PR had to be inserted, after which either SR1 or SR2 were dropped (configurations I and II). Each experiment has been repeated twice (run 1 and run 2) to verify its reproducibility. The fission chambers D1 to D4 were in L1 to L4 (reflector) respectively.

From Eq. (3) it can be seen that two input data are needed for the analysis: the initial reactivity $\tilde{\rho}_0$ and the delayed neutron data $\left(\lambda_j, \beta_j\right)$ for six families. The initial reactivity $\tilde{\rho}_0$ can be derived from the experiments by the following procedure. If the delayed neutron data are calculated for a specific state of the reactor, e.g. critical, and if the reactor is held at that state for a certain period of time, the reactivity obtained from the inverse point-kinetics procedure should be constant for that same period too. This leaves one degree of freedom to fix the initial reactivity $\tilde{\rho}_0$. After the rod drop, the count rates become rather low with quite a large noise component, which gives an erratic behaviour of the final reactivity[18]. This was eliminated by linearly smoothing the count rates and determining the value of the reactivity after the count rates were stabilized. The effective delayed neutron yields and the corresponding precursor decay constants for the six families were calculated for a critical reactor by the FX2 diffusion code[19] using a 25-group cross section library.

The above-mentioned two-dimensional diffusion code (FX2) and the 25-group nuclear data library were also used to calculate the reactivity worth of the safety rods SR1 and SR2. To this end, the lead target and the vacuum beam tube were smeared, and three XY calculations were performed: one for the unrodded core, one for the SR1 rod inserted and one for the SR2 rod inserted. In all cases an axial buckling height of 50 cm was used to get a k_{eff} of nearly unity for the unrodded core. Three-dimensional calculations were performed with the Monte-Carlo code MCNP to get some kind of calculation reference solution. The results were performed both with nuclear data from the JEF2.2 and from the ENDF-B/VI nuclear data files. Two MCNP results are given: one with cross section of lead taken from the ENDF-B/V data file, and one with the cross section of all nuclides taken from the ENDF-B/VI file. The results are given in Table VIII, together with the measurements.

As can be seen in Table VIII, the difference between the reactivity worth measured with different detectors is quite large. This is due to the fact that the disturbance of the power

profile is so large that the inverse point-kinetics analysis is not valid anymore, especially for the detectors close to the safety rods. Better values can be obtained when the influence of the spatial flux distribution on the count rates of the detectors is taken into account by spatial correction factors. The point-kinetic equations can be derived from the neutron transport equation by factorizing the neutron flux density $\phi(r,E,t)$ into a flux shape $\psi(r,E,t)$ and amplitude $n(t)$:

$$\phi(r,E,t)=\psi(r,E,t)n(t). \qquad (4)$$

One can shift the major part of the time dependence of the neutron flux density into the amplitude function by constraining the time dependence of the shape function. To this end, a second equation is needed to hold some integral value of the shape function constant in time[17]. The point-kinetics equations describe the behaviour of the amplitude as a function of time, while the shape function describes the neutron flux as a function of space.

The shape functions before and after the control rod drops were calculated using FX-2 with the 25-groups data library, and the count rate of each monitor after insertion of a safety rod was multiplied with the ratio of these shape functions. The corrected reactivity worth of the safety rods is given in Table IX, together with the calculated values.

The safety rod worth measured with monitor D2 is significantly lower than the other values, while detectors D1, D3, and D4 do give coherent results for the reactivity worth of both rods. Because detector D2 showed to be very unstable during the time of the measurement[18], its results have been discarded from the analysis. The reactivity worth averaged over D1, D3 and D4 detectors are 3909±201 pcm for SR1 and 4534±268 pcm for SR2.

As is well known, the inverse kinetic procedure provides the dynamic reactivity, this is the reactivity formed by the time-dependent neutron flux, while codes like MCNP and FX2 provide the static reactivity (the reactivity weighted by the lambda-mode flux of the perturbed

system)[17]. This means that during the rod drop, the reactivity measured by the inverse kinetics procedure differs from the calculated values. However, after the transient, when the detector count rates have stabilized, the difference between the two concepts, if any, is very small.

The reactivity worth of SR1 and SR2 calculated with MCNP (3685±67 pcm and 4523±67 pcm) agrees quite well within the margins of the experimental error. There is a difference for the reactivity worth of SR2 calculated with data from ENDF/B-V and from ENDF/B-VI (4322 pcm and 4489 pcm respectively). But both calculated values agree with the experimental values.

V. METHODS FOR SUBCRITICAL REACTORS

V.A. PNS Measurements

The power of subcritical reactors must be maintained by an external neutron source, driven in all designs of industrial systems by a particle accelerator. This fact allows the use of source intensity variations and the corresponding reaction of the reactor to monitor the reactivity of the system and to evaluate its kinetic parameters.

The complete kinetic response (without feedback) of the reactor to any arbitrary source perturbation can be derived from the experimental response of the reactor to a short pulse of the neutron source (ideally a time Dirac delta source). GENEPI allows the generation of neutron pulses with a duration shorter than 1μs, which in practical terms can be considered as instantaneous when compared to the MASURCA neutron generation lifetime ≈0.58μs (experimental value). In this way, the measurement of the neutron reaction rates versus time following a pulse of neutrons generated by GENEPI, Pulse Neutron Source or PNS experiments, allow the study of the system reactivity and some combinations of its kinetic parameters.

Figures 7 and 8 illustrate the observed counting rate of different ^{235}U FC in MUSE-4 after a (d,D) pulse from GENEPI for different reactivities[20]. These data are presented

accumulated for many neutron pulses and after subtraction of the constant level of counting produced by the delayed neutrons and the not negligible inherent source of MASURCA (Pu spontaneous fission and (α,n) reactions). For detectors in the fuel core, Fig. 7, a very simple behavior is observed for all the reactivities. A fast reaction rate increase during the source duration, is followed by a very short 5-10μs stabilization period, leading to an approximately exponential decay. The different decay constants corresponding to different reactivities allow the reactor monitoring. On the other hand the reaction rate on the reflector, Fig. 8, and on the MASURCA shielding present more complex shapes. First the reaction rate increases progressively during typically 20-30μs. Second it follows a exponential decay with a slope very similar to the core detectors in the same configuration. Finally in the cases of lower k_{eff} (k_{eff} < 0.95) the reaction rate slows its decay rate and presents additional structures after a period, that depending on the reactivity can range from 45μs for k_{eff} = 0.86 to 80μs for k_{eff} = 0.95.

The one-group point kinetic model (with one delayed family) of a reactor predicts that the time dependence of the neutron flux after a pulse of neutrons is injected is[20]:

$$n(t) = \left(\beta\lambda' e^{-\lambda' t} - \rho\alpha e^{-\alpha t}\right) \tag{5}$$

In this expression, $\lambda' = \rho\lambda/(\rho - \beta)$ and ρ is the reactivity, β is the effective delayed neutron fraction, λ is the delayed decay constant and α is the prompt decay constant, $\alpha = (\beta - \rho)/\Lambda = (1 - \rho_{\$})/(\Lambda/\beta)$. In most cases of interest GENEPI is operated at fixed frequency and amplitude, producing the same time response after each pulse. As the lowest frequency of GENEPI is 10 Hz, this provides a simplification of the above relation, since for all cases of interest then, we can make the assumption that $\lambda' t << 1$. This yields an approximation:

$$n(t) = \left(\beta\lambda' - \rho\alpha\, e^{-\alpha t}\right) \tag{6}$$

Thus, the delayed neutrons only provide a constant (with time) source of background.

The point kinetic model is unable to completely describe the observed impulse response functions, however it predicts a reactivity dependent exponential decay as observed at long times after the neutron pulse. Different approaches were followed to analyze the experimental results. Detailed Monte Carlo simulations (with MCNP) of the PNS experiments, allow the reproduction of the results and an explanation of the deviations of the point kinetic model.

The finite duration of the pulse, the time required by the neutron flux to diffuse along the reactor to the detector positions, and the time required to stabilize the neutron flux spectrum in the reflector and shielding, explain the deviation from point-kinetics during the first microseconds after the pulse

On the other hand the slow tail of neutron detections appearing at long times in reflector and shielding detectors at very subcritical MASURCA configurations, can be explained as a consequence of epithermal neutron buffering in the reflector and shielding regions[21]. These neutrons can live sufficiently long in the low absorbing reflector and shielding (half lives > 20μs), and in combination with the higher sensitivity of ^{235}U detectors to slow neutrons, they can dominate the fission counting rate when the flux reaching from the core starts to disappear. Fast neutron detectors based on the threshold fission of ^{237}Np had already been tried-out in some measurements and will be used in future MUSE-4 measurements campaigns to minimize this effect.

Fig. 9 shows the comparison of the response of detectors located in different positions of the reactor for the same core configuration[20]. Very similar evolution is observed after 30μs of the source pulse, resulting from close counting rate decay constants. The figure indicates

that with the increasing fission generations, the neutron flux is progressively approaching an asymptotic neutron flux distribution that later on evolves at the same rate in all the reactor positions. This behaviour could justify the asymptotic applicability of the point kinetics equations.

It should be noted that both the short and long time periods are strongly dependent on the position and energy distribution of the source and on the nature and relative position of the detector and, in consequence, are not representative of the reactor response to its own fission source. Only the intermediate time interval, after diffusion of the initial source and replacement by fission generated flux and before the reflector buffering becomes a secondary neutron source, has an evolution that is mainly equivalent to the intrinsic reactor kinetics.

V.A.1. Application of direct PNS methods

A first possibility for the interpretation of the PNS experiments is to apply the point kinetics relation between the exponential decay constant α and the reactor kinetic parameters (ρ, β and Λ) to obtain relations between these parameters from the value obtained for α by a exponential fit to the experimental data following the initial ramp-up of the detector reaction rate.

A set of experiments were performed to evaluate the consistency of the determination of the α decay constant from different detector positions and GENEPI operation frequencies. Table X shows this comparison for a set of experiments with different GENEPI frequencies, always in the same core configuration close to criticality[21]. Table XI presents the same comparison for a second set of data corresponding to different core configurations and a fixed GENEPI frequency (1 kHz)[20]. Despite the increasing systematic uncertainty (δ) on the α determination with decreasing reactivity, a clear compatibility of results is obtained for different GENEPI frequencies and between different detectors in the same region. However a

tendency to progressively underestimate α is observed from core to reflector and shielding detectors.

Despite the small differences between the α determination, the point kinetic equations were applied to obtain ρ, assuming a value of $\beta/\Lambda = 5800 \pm 100\ s^{-1}$ (obtained from Rossi-α measurements in a nearly critical configuration, explained later in this paper). Table XII shows the results obtained for the different detectors and core configurations. The reactivity determinations based on core and reflector detector agree within 10% whereas the shielding estimations show differences of up to 25%. The comparisons of these results to the estimation from the SM and MSM techniques show differences between 20% and 30%, however the reactivity change estimations agree to better than 5% between detectors and measurement methods close to criticality, where the SM or MSM technique is more reliable.

In summary a simple interpretation of the PNS experiments, based on the point kinetics equations allows the monitoring of reactivity changes, with precisions better than 5%, and an estimation of the actual value of the reactivity, with an agreement better than 30% respect to MSM techniques. This can be done by a simple fit to the exponential counting rate decay of detectors placed on the core or to the intermediate time interval of the reflector detectors. This approach has the risk that some bias produced by space and energy effects might be introduced in the absolute estimation of the reactivity depending on the nature and position of the detector and on the reactivity itself.

V.A.2. Application of a Method Based on Monte-Carlo Simulation

Several approaches based on detailed Monte Carlo simulations are being explored to improve the precision of the PNS evaluation of the reactivity and kinetic parameters. The aim is to remove the remaining spatial and spectral effects, and in some methods to enable the use of most of the statistics in the analysis.

According to the point kinetic model, when a pulsed neutron source is injected into the core of a subcritical reactor the neutron population decays like a pure exponential, when the delayed neutrons and the inherent source are ignored:

$$N(t) = N_0 \exp(-\alpha t) \quad (7)$$

with $\alpha = (1-k_p)/\ell$, k_p being the prompt multiplication factor and ℓ being the average generation time of a neutron. When the reactor is close to criticality (namely k_{eff}= 0.995) this decrease, which can be measured through the reaction rate of a detector located into the core, exhibits a constant slope. But for a subcriticality level relevant for an ADS (typically k_{eff}= 0.96), the slope becomes time dependent (Fig. 10).

This behaviour can be explained by the fact that when the multiplication factor is low the neutrons from the first generations become relatively more important than the ones of the later generations. That means that an average generation time is not sufficient to describe the neutron creation. We propose a more sophisticated model[24] which takes into account the distribution of the neutron generation times following a fission $P(\tau)$, τ being the time elapsed since the creation of the neutron that will give birth to the next generation. This distribution can be easily obtained by Monte-Carlo simulation for a stabilized neutron source.

From that definition we deduce that

$$\int P(\tau) d\tau = k_p \quad (8)$$

and thus we can normalise $P(\tau)$ to k_p = 1. With that normalised distribution $P'(\tau)$, we have access to the number of neutrons in the core at any time for any k_p value, summing the contribution of each generation:

$$N_{kp}(t) = k_p P'(\tau) + k_p^{\,2} P'(\tau)*P'(\tau) + k_p^{\,3} P'(\tau)*P'(\tau)*P'(\tau) + \ldots \quad (9)$$

where * denotes the convolution operator. The decrease rate $\alpha_{kp}(t)$ can then be calculated for different k_p values from the logarithmic derivative:

$$\alpha_{kp}(t) = \frac{1}{N}\frac{dN}{dt} \quad (10)$$

and compared to the α (t) obtained from the experimental N(t) spectrum, the one fitting the best the experiment giving the estimation for the k_p value of the reactor. This method has been applied to the spectra shown in Fig. 10. The α (t) curves obtained from the fits of these spectra are shown together with relevant calculated $\alpha_{kp}(t)$ curves in Fig. 11. With the U5 chamber the k_p values of the core are found bounded by 0.990 and 0.993 for the assembly close to the criticality, and by 0.955 and 0.960 in the other case. They are in rather good agreement with the k_p values deduced from the SM measurements with $k_p = k_{eff}(1 - \beta)$: 0.9922±0.0003 for the configuration III and 0.9563±0.0025 for the configuration V.

The α (t) obtained from the ^{3}He counter exhibits a slightly different behaviour compared to the U5 data. This can be explained by the location of the counters: the U5 chamber is in the middle of the fuel zone while the ^{3}He counter is close to the reflector and thus submitted to more low energy neutrons. To improve measurements in such locations the use of detectors with energy threshold (like ^{237}Np, ^{238}U or ^{232}Th FC for instance) is required.

This method is very promising as it can include the contribution from the measurement made in the first tens of microseconds after the pulse, where the counting rate is still high, in the estimation of k_p value, reducing the dependency on later times after the pulse where the statistic might be poor. Moreover it has the potentiality to reduce the absolute bias

of the estimation of k_{eff}, from the simple point kinetic model, where it has been shown in the previous section that the agreement between the theoretical α value given by the point kinetics model and the direct exponential fits to the experiments can have deviations from 5% to 25% depending on the detector location.

This method and its robustness are detailed in Ref. 24.

V.A.3. Determination of $\rho(\$)$

A different application of the direct point kinetics has been used to extract $\rho_\$$ without the need of any external parameter. This method, also known in literature as the Sjöstrand method[25], is based on the determination of the ratio between the prompt and delayed areas, For a single isolated pulse the ratio of the integrals of the prompt *PN* and delayed components *DN* equates to $PN/DN=-\rho/\beta_{eff}=\rho_\$$. In the experiments at MUSE, the frequency is higher than the inverse of the delayed neutrons precursors lifetime and in consequence the delayed neutrons of many preceding pulses pile up to form a base level for the prompt component of each pulse. Several minutes after a fix frequency and intensity have been set in GENEPI, the base level of detection rate due to the delayed neutrons reach its asymptotic value and remains constant unless the frequency or the intensity are modified. GENEPI stability is better than 1% in both parameters. In addition, the inherent source due to the Pu spontaneous fission and the (α,n) reactions also contribute to the value of the constant base level.

To obtain the ratio PN/DN in the MUSE experiments, first the inherent source has to be subtracted. This has been done either by a calibration, measuring without external source, or by comparing two measurements with different frequencies. After this subtraction, the distribution of the counting rate between two pulses (accumulated for a large number of pulses) is analysed. The delayed neutron contribution is obtained by multiplication of the constant level observed at the end of the GENEPI period times the period duration. The prompt integral is obtained as the total number of counts minus the delayed neutron

contribution. Table XIII shows the results for several MUSE configurations and can be compared with Table XII .

The agreement of the different reactivity estimations from different inherent source subtraction and frequency combinations is better than 20%. The comparison of different detectors is also better than 20% in all cases and in many cases better than 5%. Finally the results have a small tendency to calculate higher ρ values than the direct PNS fitting, with differences below 10%.

V.B. Noise Measurements

V.B.1. Rossi-α Method

The Rossi-α technique[26] is based on the statistical nature of the fission-chain process. Using a coincidence acquisition system, the rationale is to experimentally determine the probability distribution of detecting neutrons from the same chain. The Rossi distribution, related to the correlation function of neutron detection time series, can be derived theoretically through a birth-to-death probability balance equation, namely the backward master equation[27]. Here, we only consider the following Rossi distribution p_{rossi} for a point kinetic model without delayed neutrons:

$$p_{rossi}(\tau)dt_g dt_c = \varepsilon_g F_0 dt_g (\varepsilon_c F_0 dt_c + \frac{\varepsilon_c D}{2\alpha\Lambda^2} dt_c e^{-\alpha\tau}), \quad \tau = t_c - t_g \tag{11}$$

The above expression can be heuristically derived. The Rossi-α experiment is as follows. There are two input channels: a trigger channel with detection efficiency ε_g and counting channel with efficiency ε_c. Those two channels can be provided by either a single detector (auto-correlation) or two separate detectors (cross-correlation). A time gate ΔT divided in bins of width dt_c is opened at a certain time t_g by a pulse from the trigger channel. Some bins dt_c corresponding to the elapsed time between the occurrence of a pulse from the counting channel at t_c and this of the original trigger pulse are then incremented. Since a

timemarking acquisition system is capable of recording all the events of any detector and thus makes possible an offline data reduction, a time gate of width ΔT is opened for each trigger pulse. This data processing is referred as to the Rossi-α type I in the literature. According to the above equation, the number of coincidence counts n_{rossi} in a bin i corresponding to the lag $t = idt_c$ is given by:

$$n_{rossi}(t) = n_{rand} + n_{corr} e^{-\alpha t} . \tag{12}$$

The uncorrelated or random component n_{rand} is:

$$n_{rand} = N_g \varepsilon_c F_0 dt_c \tag{13}$$

where $N_g = \varepsilon_g F_0 T$, the number of time gates, is proportional to the acquisition duration T. The correlated component n_{corr} is:

$$n_{corr} = N_g \varepsilon_c \frac{D}{2\alpha\Lambda^2} dt_c \quad . \tag{14}$$

Assuming that the number of coincidence counts n_{rossi} approximately follows a Poisson distribution, its standard deviation σ_{nrossi} is:

$$\sigma_{nrossi}(t) = \sqrt{n_{rossi}(t)} . \tag{15}$$

We have performed Rossi-α experiments in the MUSE-4 Reference core (configuration VII, GENEPI off) with the pilot rod down. The corresponding reactivity is ρ_{REF} = -120 ± 7 pcm (as measured by RD techniques). We are presenting in this section the different α-values obtained with the Rossi method. Eight runs of 2800 s were done with our time marking acquisition system. The dwell time was set to 100 ns. It is important to note that

we had to move the most efficient monitors to the reflector region for noise experiments in order to obtain sufficient count rates.

Rossi-α (and Feynman-α for that matter) experimental data series are analyzed with the use of a least squares fitting method. For evaluating the goodness of fit, one uses graphical and numerical indicators. The scatter plot should not display any pattern or trend. In other words, the residuals (the differences between the response values and the predicted response values should be random errors. Classically, a good fit is indicated by the square of the correlation coefficient r^2 being nearly unity. This parameter measures how successful the fit is in explaining the variation of data. The root mean squared error, *RMSE*, is another statistic closely related to the scatter plot since it is defined as the square root of the summed square of residuals divided by degrees of freedom. One hopes for generally low values of the *RMSE*.

The Rossi-α fitting model is $p(t)=n_{rossi}(t)/n_{rand}$. The domain of fit spans from 10μs to 1ms since in the case of cross-coincidence the lag t is not likely to be less than 10μs. An example is shown in Fig. 12, where we show the Rossi-α curve and the residuals.

In Table XIV we show fit results for different detector pairs located in different parts of the core. The detectors D3 and D4 in the reflector (in L3 and L4 respectively), and D8 and D5 in the core (in L7 and L5 respectively) do not allow us to accurately estimate α-values because their poor efficiency leads to poor statistics. We also note that while the standard errors are about 1% for detectors D10 and D11 (located in the reflector in L1 and L2), the discrepancies between α-values are quite large. For the moment, lacking further information, we express this variability as a type-B uncertainty[b] as follows:

$$\delta = \frac{\alpha_{\max} - \alpha_{\min}}{2}. \qquad (16)$$

[b] Following the convention of NIST, a type-B uncertainty is one of which we don't know the probability law.

Thus, we can give our best estimate of α and associated uncertainty as follows[21]:

$$\alpha_{RA} = \overline{\alpha} \pm \delta = 8017 \pm 673\ s^{-1}\ (8.4\%).$$

As another Rossi-α example, we show the distribution for configurations VII and VII with the PR inserted to be very close to criticality[23] (ρ= -120 pcm and ρ= -20 pcm) in Fig. 13. Due to the high level of the inherent source, the signal to noise ratio is extremely small[c], around 0.1%, which has made it necessary to share the counts of the two detectors used in the experiments as if they were actually one. This is a good assumption since both detectors have approximately the same mass and they are located in symmetrical positions.

The first thing that can be observed, and which happens for both configurations, is that it is necessary to analyze the exponential decay after a short delay time of around 30 or 40 μs.

Although this is a deviation from the assumed point kinetics, it must be taken into account that the detectors are not placed in the fuel region but in the reflector, so there is the time the neutrons need to arrive at the detector (as is also seen in the case of the pulsed neutron source experiments).

When comparing the different exponential decays the different reactivity levels for the two different configurations can be clearly observed in the values of the prompt decay constant, α. This feature can be used for reactivity off-line calibration, however, very long acquisitions would be required for a more subcritical situation.

Results from additional measurements are shown in Table XV. Included in this series is a measurement made at a subcritical level of -3795 pcm (configuration VI) to analyze applicability of the method for realistic ADS conditions.

Table XV shows that the spread between measurements for the same experimental conditions is almost negligible, whereas a discrepancy between the results for two symmetrical positions measured with the same detector type (uranium-235 fission chamber)

[c] As also seen on Fig. 12.

can be observed. This is the same behaviour as noted above, and again for the moment we are assuming this is a type-B uncertainty (again of the order of 8%). However, further investigations will have to address whether this difference is due to different reactor physics at these positions or results from detector and/or electronics characteristics.

Fig. 14 presents the results for a deep subcritical configuration. Very poor statistics was collected on this experiment. New measurements are scheduled to collect additional statistics at this subcriticality level.

V.B.2. Feynman-α

Feynman and de Hoffman[28] showed that the number of counts c in a time gate ΔT deviates from a Poisson distribution because of the fluctuations of the neutron population driven by the fission chain process. For a given time gate ΔT, the deviation is measured by the y-value defined as:

$$y = \frac{\text{var}\,iance}{mean} - 1 = \frac{\langle c^2 \rangle - \langle c \rangle^2}{\langle c \rangle} - 1 \tag{17}$$

That expression can be generalized to the case of two different detectors k and l with detection efficiencies ε_k and ε_l, respectively:

$$y_{k,l}(\Delta T) = \frac{\langle c_k c_l \rangle - \langle c_k \rangle \langle c_l \rangle}{\sqrt{\langle c_k \rangle \langle c_l \rangle}} - \delta_{k,l} \tag{18}$$

where $\delta_{k,l}$ is the Kronecker symbol. For $k \neq l$, the numerator of the y-value is a covariance term.

The y-value is related to the Rossi distribution through the average number of pairs counted in a time gate ΔT:

$$\frac{c_k(c_l-\delta_{k,l})}{2}=\int_0^{\Delta T}dt_c\int_0^{t_c}dt_g\ \ p_{rossi}(t_c-t_g) \tag{19}$$

One thus obtains the following expression for the *y*-function assuming a point kinetic model and considering prompt neutrons only:

$$y_{k,l}(\Delta\mathrm{T})=\frac{\sqrt{\varepsilon_k\varepsilon_l}D}{\alpha^2\Lambda^2}\left(1-\frac{1-e^{-\alpha\Delta\mathrm{T}}}{\alpha\Delta\mathrm{T}}\right) \tag{20}$$

The standard deviation σ_y of the *y*-value can be approximately derived from those of the sample variance and mean of the normal distribution:

$$\sigma_y=\frac{1+y_{k,l}}{\sqrt{N}}\sqrt{\frac{1+y_{k,l}}{m_{k,l}}+2},\quad m_{k,l}=\sqrt{\langle c_k\rangle\langle c_l\rangle} \tag{21}$$

where *N* is the number of samples (i.e. the number of counts) for a given time gate ΔT.

The *y*-value can be sometimes negative because of either a dead time effect at high counting rates[28-30] or a poor statistics in a system with neutron generation times Λ less than 10 μs[30]. Assuming a non-paralyzable counting system, Yamane proposed the following improved formula in Ref.29:

$$y_{k,l}^{d}=y_{k,l}-2Rd\delta_{k,l} \tag{22}$$

where *d* and *R* are the total dead time and the counting rate associated to a neutron channel, respectively. While we have not completely analyzed our system's dead-time, we have found that it is necessary to add a positive constant term to the covariance-to-mean model in order to

successfully fit the experimental data series. We show the results after the correction has been made in Table XVI.

The α-estimates obtained with the detectors D8 and D5 are rejected because of their poor statistical indicators. For the other detectors, the discrepancies between α-values are quite large even if the standard errors are less than 2%. Their variability is measured in the same manner as the Rossi-α case. Thus the best estimate for a reactivity level of a –120 pcm is[21]:

$$\alpha_{FA} = \overline{\alpha} \pm \delta = 8244 \pm 688 s^{-1} (8.3\%)$$

In Fig. 15, the Feynman-α distributions for configurations with a reactivity of ρ = -120 pcm is shown[23].

We note that the variance to mean ratio is negative. However, after applying corrections[31], we can remove this problem and the experimental results can be described by the classical model. The α-values extracted from the Rossi- and the Feynman- α technique are coherent within the uncertainties. This might be explained taking note that the Feynman-α expression can be obtained by integrating the Rossi-α formula.

The Feynman-α distribution for the configuration VI (ρ = -3795 pcm) is shown. As in the previous cases, the correction of equation (22) had to be introduced before fitting. In addition the first points were discarded from the fit. The value of α is different enough to be used for reactivity monitoring. However, and as it happened in the pulsed neutron source experiments, trying to extract a direct value of the reactivity from α can be considered as a first approximation and several corrections must be applied in order to give a precise value.

V.B.3. Frequency analysis[32]

Applying the Fourier Transform operator , $\int d\tau \exp(-iw\tau)$, to the auto and cross correlation function described in section V.B.1, we get the expressions for the auto- and cross-power spectral density functions:

$$APSD_{D_gD_g} = \frac{\varepsilon_g^2 D}{2\alpha\Lambda^2} F_0 \frac{1}{\left(\alpha^2 + w^2\right)} + \varepsilon_g^2 F_0^2 \tag{23}$$

$$CPSD_{D_gD_c} = \frac{\varepsilon_g \varepsilon_c D}{2\alpha\Lambda^2} F_0 \frac{1}{\left(\alpha^2 + w^2\right)} \tag{24}$$

From the break frequency of both spectral densities, the α-value of the system can be obtained. Because the signal to noise ratio is very low, we cannot extract the reactor frequency from the auto power spectral density and we used only the cross power spectral density.

The measurements were performed in continuous current mode using a pair of high efficiency fission chambers (D10 and D11) placed in positions L1 and L2. The fission chamber current is passed through a high bandwidth current to voltage converter and amplifier is used to record the fission chamber current. The amplifier includes a high-pass filter to remove the high voltage DC part in the signal. After additional amplifiers and anti-alias filters the signal is sampled and recorded by PC. Because we operate in current mode no dead time correction is applicable. Measurements at deeply subcritical (configuration VIII, about -15000 pcm) were performed in order to get the electronic transfer function assuming that in the frequency bandwidth used (70Hz, 4kHz) the system frequency cannot be measured because it is higher.

Here two detectors with high efficiency were located at the position L1 and L2 in the reflector. The increased efficiency together with the relatively high neutron flux level at these positions allowed us to perform the measurements in continuous current mode. The Fig. 17

shows the CPSD between the detectors after a measurement of 50 minutes at a power of 20 Watts. From the APSD of either detector, it was not possible to get an accurate value for α because of the strong inherent spontaneous fission source, which leads to a very low signal to noise ratio. The α obtained from the CPSD, however, corresponds reasonably well with the values obtained with the pulse-mode experiments.

V.B.4. Summary of Noise Methods

In the previous sections, we presented some preliminary results from Rossi-α, Feynman-α and CPSD noise measures.

In the Rossi-α, we showed statistical fits with correlation coefficients on the order of 0.95, and least squares residuals on the order of 1% for each individual measurement. However, comparison among measurements exhibits a greater spread than would be obtained by true 1% measurements, so we have assigned Type-B uncertainties on the order of 8%. This is not entirely unexpected as the signal to noise (S/N) ratio of our measurements are typically on the order of 0.1%. Most of the measurements were performed close to critical, but we did make some around k=0.96. While the statistics are very poor, it was possible to extract an α value. However, more work has to be performed before we can truly assess the uncertainties of such measurements at more sub-critical levels.

The conclusions from our Feynman-α measurements are essentially the same as the Rossi-α (as they should be given the relation between the two). Again, we have poor measures without using high efficiency detectors, and we see the same 8% spread in comparing separate measures. At k=0.96 an α was inferred, but again we must assess the uncertainties.

Finally, CPSD measures demonstrated the inference of α through the break frequency. As in all cases, the low S/N ratio is a problem.

In summary, the Rossi-α, Feynman-α, and CPSD methods do yield consistent results. The conditions are less than ideal because of the need for very high efficiency chambers and the inherent background fission rate in MASURCA. However, it seems that our measures are consistent to the order of 10-15% at this stage which may be adequate for off-line calibration monitoring of a system at deep subcritical levels.

V.C. Spectroscopy Measurements

Neutron spectrometry in fast neutron reactors is not trivial considering spectra are continuous, ranging up to a few MeV and especially because the neutron flux is very large even in a small research reactor (about 10^6 to 10^8 n/cm^2/s, depending on the operating conditions). We recorded the core neutron spectrum for the first time with a ^{3}He proportional counter which gives the neutron energy E_n through the relation $E_n = E_{detected} - Q$, and whose energy calibration is easy due to the thermal neutron peak at Q = 764 keV. For such measurements the response function of the detector, which is not a monodimensional bijection due to the finite size of the counter and to the competition between (n,p) reactions and elastic scattering, must be firstly obtained with monoenergetic neutrons. Once this response function versus the neutron energy is known it is possible to extract the neutron spectrum from the experimental spectrum recorded in the core by an iterative subtraction method[33]. The result, obtained from a measurement made in the fuel zone close to the reflector and for k_{eff} = 0.96 (configuration V), is shown compared to the neutron spectrum simulated with the Monte Carlo code MCNP-4C in the Fig. 18. The overall agreement is rather good up to 600 keV, which represents about 75% of the flux. Around 450 keV an underestimation is seen which is inherent to our subtraction method which fails to fully reproduce the flux depression due to the oxygen resonance around 400 keV: it induces an overestimation for a few following lower energy bins. The extraction method is still being improved. Above 600 keV the extraction of the spectrum was not possible as the experimental

spectrum is spoilt by counting rate due to background reactions in the counter itself which has the same order of magnitude than the neutron reactions on ^{3}He. This is occurring because the ^{3}He pressure in the counter is very low. To solve this problem the ^{3}He pressure will be slightly increased and a background measurement with a ^{3}He free counter will be systematically made and subtracted from the spectrum.

We aim to be able to measure neutron spectra up to MeV energies. This technique will allow us to validate our simulations in a subcritical medium.

VI. CONCLUSIONS

During the last 2 years, the MASURCA facility has been set-up to perform the MUSE-4 experimental program, including the installation of an advanced neutron generator (the GENEPI deuteron accelerator), the installation of new calibrated detectors and electronics, new data acquisition, new auxiliary systems and, last but not least, obtaining the licence to operate in critical and a range of subcritical configurations coupled with the D-D and D-T external neutron source.

Indeed MASURCA reached its first criticality in the MUSE-4 Reference configuration on January the 10th 2001. In addition, exploratory configurations with subcriticalities ranging from k_{eff}=0.85 to closer to critical (20 pcm) were studied with the Pu inherent source and with the D-D source supplied by GENEPI.

The systematic characterization of the properties of the MUSE-4 configurations is progressing. In this paper the spatial distribution of the neutron fluence (^{235}U reaction rate), several spectral indices at different positions, activation measurements and the first evaluation of the critical reference configuration based on the SM and MSM techniques, were presented.

In addition the kinetic behavior of several subcritical MASURCA configurations operated with a pulsed D-D neutron source have been studied, testing several techniques for reactivity monitoring and evaluation.

The point kinetic reactor model predicts an exponential decay of the fluence after a pulse and a linear relation between the decay constant (of any detector) and the reactivity. The experiments presented in this paper show that a simple exponential relation cannot be assumed to be valid in all cases, especially for detectors in the shielding and to a certain extent in the reflector. For short times after the neutron pulse (< 20μs), different detectors present different time response functions, not necessarily exponential. On the other hand, it has been shown that after a first period after the neutron pulse (ranging from 10μs to 50μs for different reactor configurations) the fundamental mode behavior of the reactor is progressively approached. The results presented show that, at least, it appears to be a one-to one relation between the reactivity and the exponential decay constant, in the intermediate time range, of each detector (position and type). In addition, it has been shown that a precision better than 30% in the absolute value of the reactivity can be achieved by this method. On the other hand, Monte Carlo simulations indicate the presence of systematic errors in the exponential decay at long times (> 100μs) when the detector is based on the ^{235}U fission. This effects are enhanced by the large fission probability of the epithermal neutrons "*accumulated*" on the reflector.

The full information contained in the PNS experiments, can only be extracted with the help of detailed computer simulations that allow to take into account the spatial and spectral effects affecting the different detectors. Several strategies are being tested for this purpose. One of these methods presented in this paper, based on the use of the first μs after the neutron pulse, has given very promising results for the configurations studied.

Finally several noise techniques, Rossi-α and Feynman-α, have also been explored, as complementary methods for reactivity monitoring and calibration. The results obtained are consistent results with other methods and calculations for reactivity and dynamic parameters such as β/Λ.

In addition we have performed preliminary neutron spectroscopy measurements. We are in the process of analyzing the suitability of this technique in fast reactor systems. It is too early to draw definitive conclusions.

Most of the subcritical measurements presented in this paper were performed in largely deformed reactor configurations. Consequently the previous conclusions require confirmation from other configurations corresponding to the same reactivity levels. Indeed the MUSE-4 program foresees these measurements in 4 configurations (SC0, SC2, SC3 and SC3 with a lead zone) till the beginning of 2004, that will allow us to perform the previously described measurements, make comparisons at different reactivity levels, and to evaluate the uncertainties.

ACKNOWLEDGMENTS

The authors are very grateful to the CEA MASURCA operating and maintenance teams and also the ISN GENEPI accelerator technical team for their availability and help during the running of experiments.

This work is partially supported by the 5th Framework Programme of the European Commission through the contract FIKW-CT-2000-00063, by GEDEON (French concerted research organizations investigating new options for waste management) and by ENRESA.

REFERENCES

1. M. SALVATORES et al., "Role of accelerator-driven systems in waste incineration scenarios", Global'97

2. G.PERRET and J.-F.LEBRAT, CEA CPSD measurements not yet published, private communication, 2002.

3. M. SALVATORES et al., "MUSE-1 : A first experiment at MASURCA to validate the physics of sub-critical multiplying systems relevant to ADS", Second International Conference on Accelerator-Driven Transmutation Technologies and Applications. KALMAR, SWEDEN, June 3-7, 1996.

4. R. SOULE et al., "Validation of neutronic methods applied to the analysis of fast subcritical systems: The MUSE-2 experiments", Global'97, YOKOHAMA, October 5-10, 1997.

5. J.F. LEBRAT et al., "Experimental Investigation of Multiplying Subcritical Media in presence of an External Source : the MUSE-3 Experiment ", ADTTA'99, Prague, may 1999.

6. G. ALIBERTI « Caractérisation Neutronique des Systèmes Hybrides en Régimes Stationnaire et Transitoire »
   PHD Thesis, Université Louis Pasteur de Strasbourg (France), October 2001.

7. J.Y. Doriath et al., "ERANOS1: The Advanced European System of Codes for Reactor Physics Calculations", International Conference on Mathematical Methods, Karlsruhe, Germany, 1993.

8. G. ALIBERTI, G. RIMPAULT, R. JACQMIN, J.F. LEBRAT, P.J. FINCK, G. IMEL, A. RINEISKI, P. RAVETTO, J.C. SENS, “Dynamic Measurements and Control of an Accelerator Driven System (ADS)”, PHYSOR-2002, Seoul, Korea, Oct 7-10, 2002. Conference Proceedings (CD-Rom), ANS 2002, 12C-03.

9. G. PALMIOTTI, E.E. LEWIS, C.B CARRICO, “VARIational Anisotropic Nodal Transport for Multidimensional Cartesian and Hexagonal Geometry Calculations”, ANL-95/40, Argonne Nationzl Laboratory, Reactor Analysis Division, October 1995.

10. J.F. BRIESMEISTER, “MCNP – A General Monte Carlo N-Particle Transport Code”, Los Alamos National Laboratory Report LA-12625, Los Alamos, USA (1993).
"MCNP-4C General Monte Carlo N-Particle Transport Code", Los Alamos, LA-13709-M, (2000).

11. M. PLASCHY, C. DESTOUCHES, C. DOMERGUE, H. SERVIÈRE, P. CHAUSSONNET, J.M. LAURENS, R. SOULE, G. RIMPAULT and R. CHAWLA, “Foil Activation Studies of Spectral Variations in the MUSE4 Critical Configuration,” PHYSOR-2002, Seoul, Korea, Oct 7-10, 2002. Conference Proceedings (CD-Rom), ANS 2002, 12C-04.

12. J. ROWLANDS ET AL., “The JEF-2.2 Nuclear Data Library”, NEA/OECD - JEFF Report 17, Paris, France (2000).

13. D. VILLAMARIN, R. SOULE AND E. GONZALEZ, “Benchmark on Computer Simulation of MASURCA Critical and Subcritical Experiments (MUSE4 BENCHMARK)”, NEA/OECD - WPPT(2001)5, Paris, France (2001).

14. M. PLASCHY, O.P. JONEJA, G. RIMPAULT, C. DESTOUCHES and R. CHAWLA, “Investigation of local spectral differences between critical and driven subcritical configurations in MUSE4, ” Proc. 7th Exchange meeting on Actinide and Fission Product Partitioning & Transmutation, Jeju, Korea, Oct 14-16, 2002, Proceedings to be published.

15. J.J. DUDERSTADT and L.J. HAMILTON, *Nuclear Reactor Analysis*, John Wiley&Sons, Inc., (1976)

16. J.E. HOOGENBOOM and A.R. VAN DER SLUIJS, "Neutron Source Strength Determination for On-Line Reactivity Measurement", *Annals of Nuclear Energy,* **15,** pp.553-559 (1988).

17. KARL O. OTT and ROBERT J. NEUHOLD, *Introductory Nuclear Reactor Dynamics*, American Nuclear Society, (1985)

18. J.L. KLOOSTERMAN, Y. RUGAMA, M. SZIEBERTH, and C. DESTOUCHES, "Measurement and Calculation of Control Rod Worths in MASURCA", PHYSOR-2002, Seoul, Korea, Oct 7-10, 2002. Conference Proceedings (CD-Rom), ANS 2002, 13C-03.

19. R.A. SHOBER, T.A. DALY, and D.R. FERGUSON, "FX2-TH: A Two-Dimensional Nuclear Reactor Kinetics Code with Thermal-Hydraulic Feedback", Argonne, Illinois 60439, (1978).

20. D.VILLAMARIN and E.GONZALEZ-ROMERO, “First CIEMAT Measurements of the MUSE-4 Kinetic Response”, PHYSOR-2002, Seoul, Korea, Oct 7-10, 2002. Conference Proceedings (CD-Rom), ANS 2002, 13C-04.

21. C.JAMMES, G.PERRET, G.IMEL, “First Muse-4 Experimental Results Based on Time Series Analysis”, PHYSOR-2002, Seoul, Korea, Oct 7-10, 2002. Conference Proceedings (CD-Rom), ANS 2002, 12C-02.

22. D.VILLAMARIN ET AL.,”Thermal Contribution in the Time Response of a ^{235}U Detector in the Reflector Zone of MASURCA Core”, CEA Internal Report, CEA-NT/SPEx/LPE/01-048 (2001).

23. D. Villamarin, G. Perret, E. Gonzalez, R. Soule, C. Jammes, G. Imel, C. Destouches, P. Chaussonnet, J.M. Laurens, G.M. Thomas, P. Fougeras, G. Bignan, “ First measurements of the kinetic response of the MUSE-4 fast ADS mock-up to fast neutron pulse “, Proc. 7th Exchange meeting on Actinide and Fission Product Partitioning & Transmutation, Jeju, Korea, Oct 14-16, 2002, Proceedings to be published.

24. F.PERDU, J.M.LOISEAUX, A.BILLEBAUD, R.BRISSOT, D.HEUER, C.LEBRUN, E.LIATARD, O.MÉPLAN, E.MERLE, H.NIFENECKER, J.VOLLAIRE, “Prompt reactivity determination in a subcritical assembly through the response to a dirac pulse”, *Progress in Nuclear Energy*, **42** (2003) 107.

25. E.GARELIS, « Survey of pulsed neutron source methods for multiplying media », Proceedings of the Symposium on Pulsed Neutron Research, AIEA, Karlsruhe, May 10-14, 1965.

26. R. E. UHRIG, Random Noise Techniques in Nuclear Reactor Systems, Ronald Press, New York (1956).

27. G. I. BELL, "On the Stochastic Theory of Neutron Transport", *Nucl. Sci. Eng.*, **21**, pp. 390- (1956).

28. R. P. FEYNMAN, ET. AL., "Dispersion of the Neutron Emission in U-235 Fission", *J. Nucl. Energy,* **3**, pp.64-69 (1956).

29. Y. YAMANE, "Feynman-α Formula with Dead Time Effect for a Symmetric Coupled-Core System", *Ann. Nucl. Energy,* **23**[12], pp.981 (1996).

30. S. K. SRINIVASAN and D. C. SAHNI, "A Modified Statistical Technique for the Measurement of α in Fast and Intermediate Reactor Assemblies", *Nucleonik,* **9**[3], pp. 155-157 (1967).

31. Y. KITAMURA ET AL., General Formulae for the Feynman-α Method with the Bunching Technique", *Ann. Nucl. Energy,* **27**, pp.1199-1216 (2000).

32. Y. RUGAMA, J.L. KLOOSTERMAN and A. WINKELMAN, "Preliminary Measurements of the Prompt Neutron Decay Constant in MASURCA", *Progr. Nucl. Energy*, 43, pp. 421-428 (2003).

33. A.BILLEBAUD, R.BRISSOT, D.HEUER, M.KERVENO, C.LE BRUN, E.LIATARD, J.-M.LOISEAUX, O.MÉPLAN, E.MERLE, F.PERDU, J.VOLLAIRE, C.DESTOUCHES, P.CHAUSSONNET, J.-M.LAURENS, "The MUSE-4 Experiment: Prompt Reactivity and Neutron Spectrum Measurements", PHYSOR-2002, Seoul, Korea, Oct 7-10, 2002. Conference Proceedings (CD-Rom), ANS 2002, 13C-01.

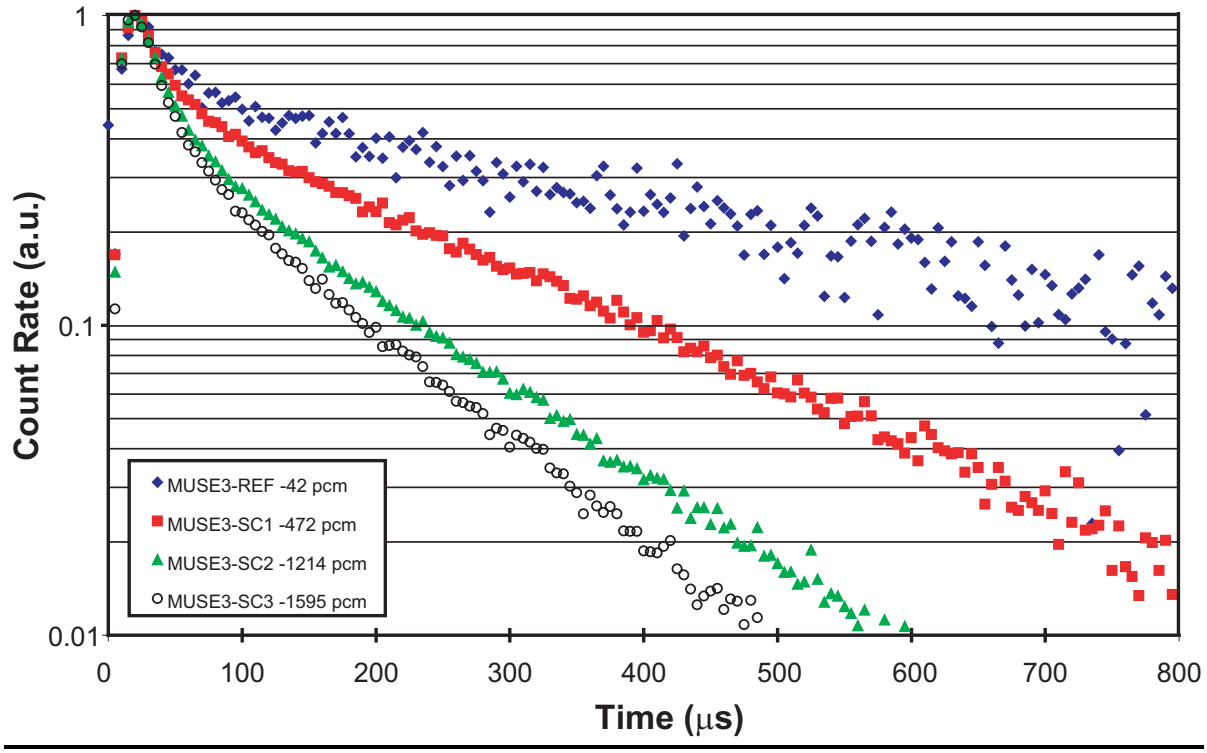

Fig. 1. Pulsed Neutron Source measurements in MUSE-3 for different subcritical levels.

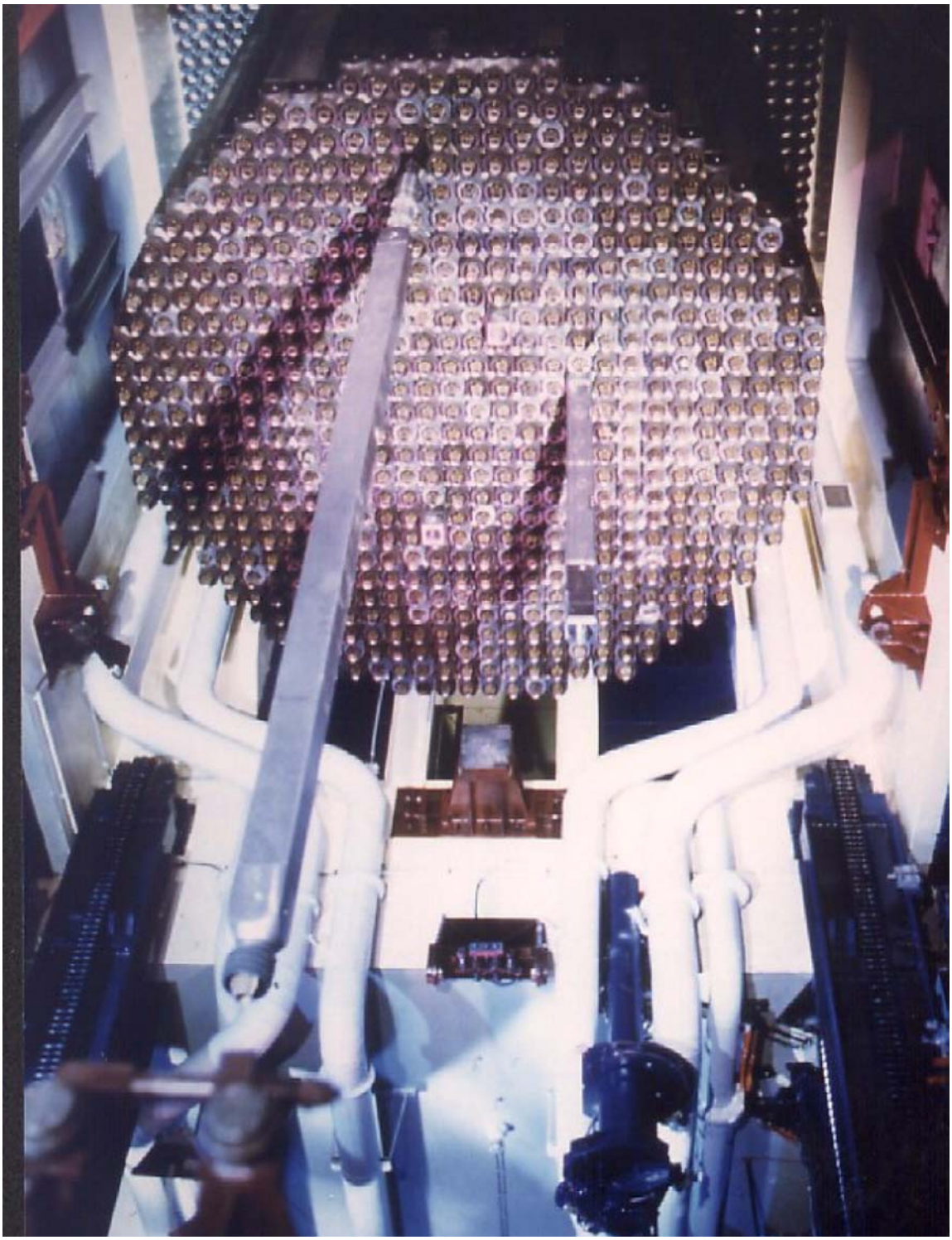

Fig. 2. MASURCA core loading from the bottom.

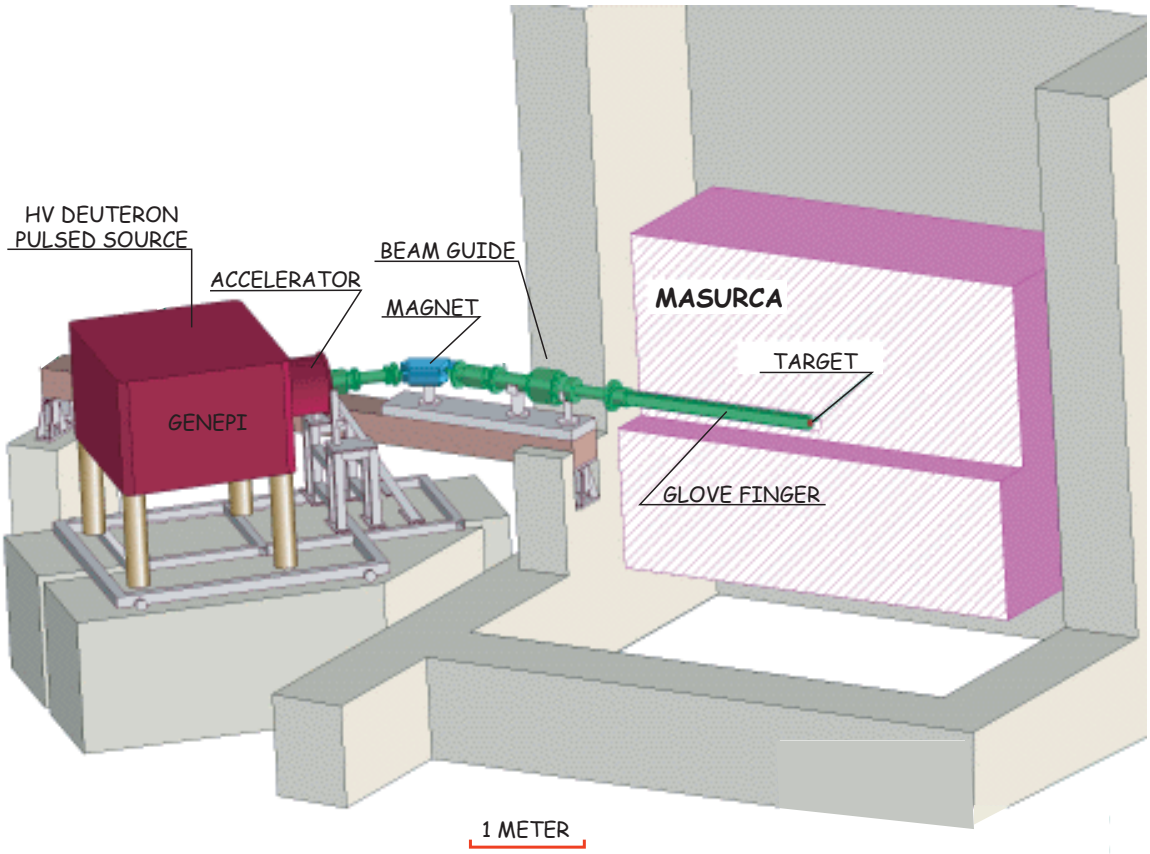

Fig. 3. The GENEPI accelerator coupled to MASURCA.

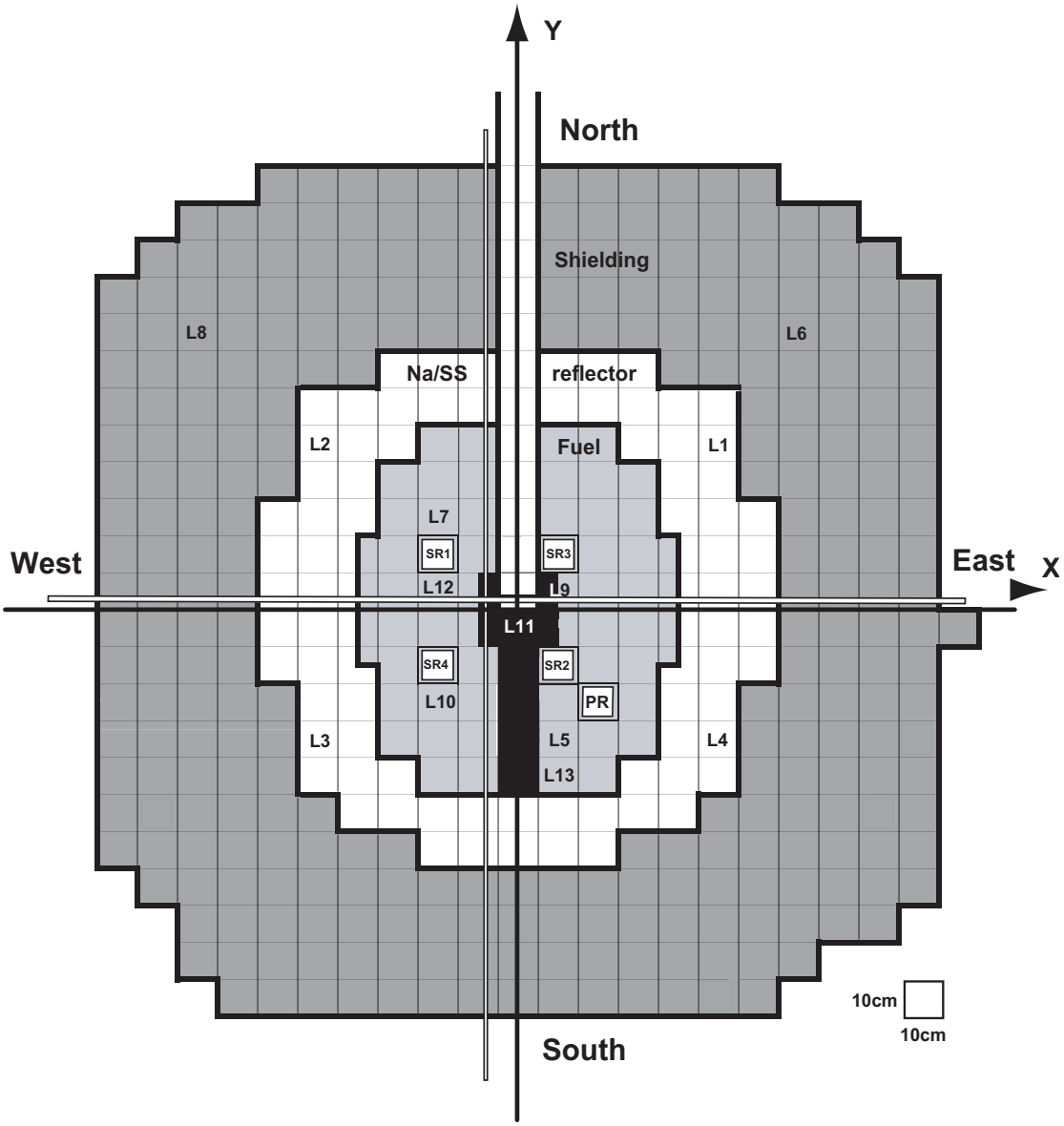

Fig. 4. XY cut of the MUSE-4 Reference critical configuration at the core median plane with measurement locations.

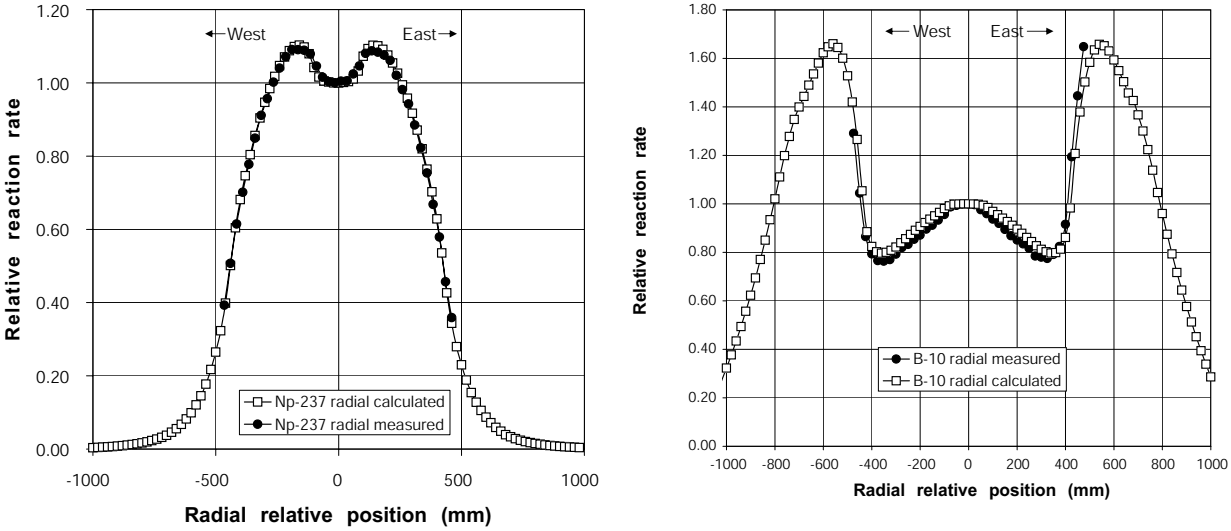

Fig. 5. Radial traverses thermal and threshold reaction rates. Left (a): ^{237}Np, right (b): ^{10}B.

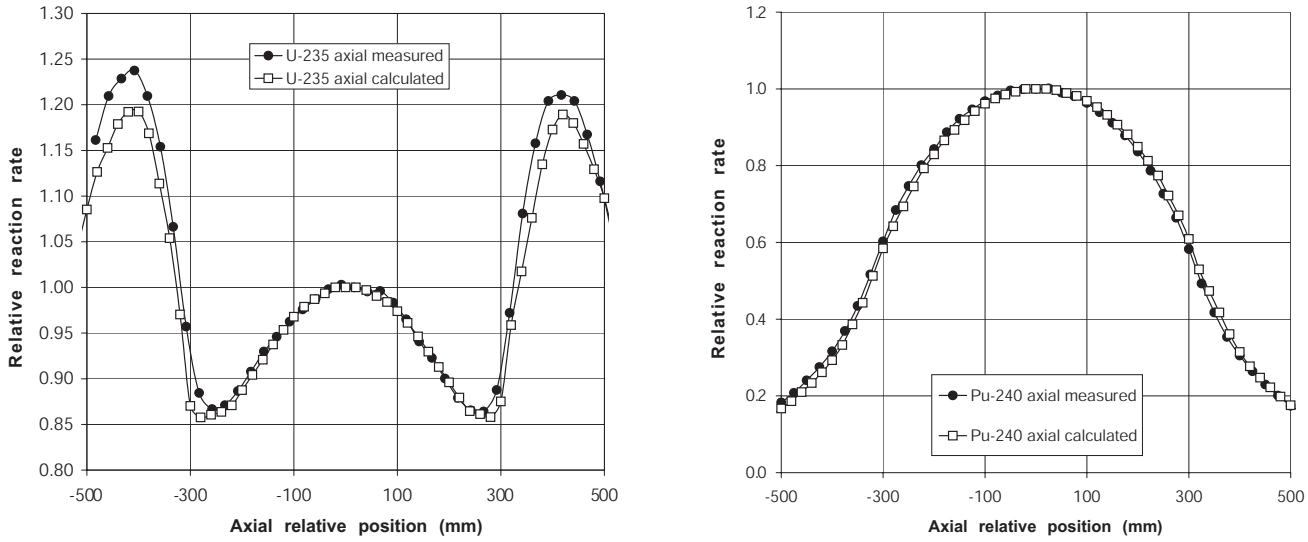

Fig. 6. Axial traverses thermal and threshold reaction rates. Left (a): ^{235}U, right (b): ^{240}Pu.

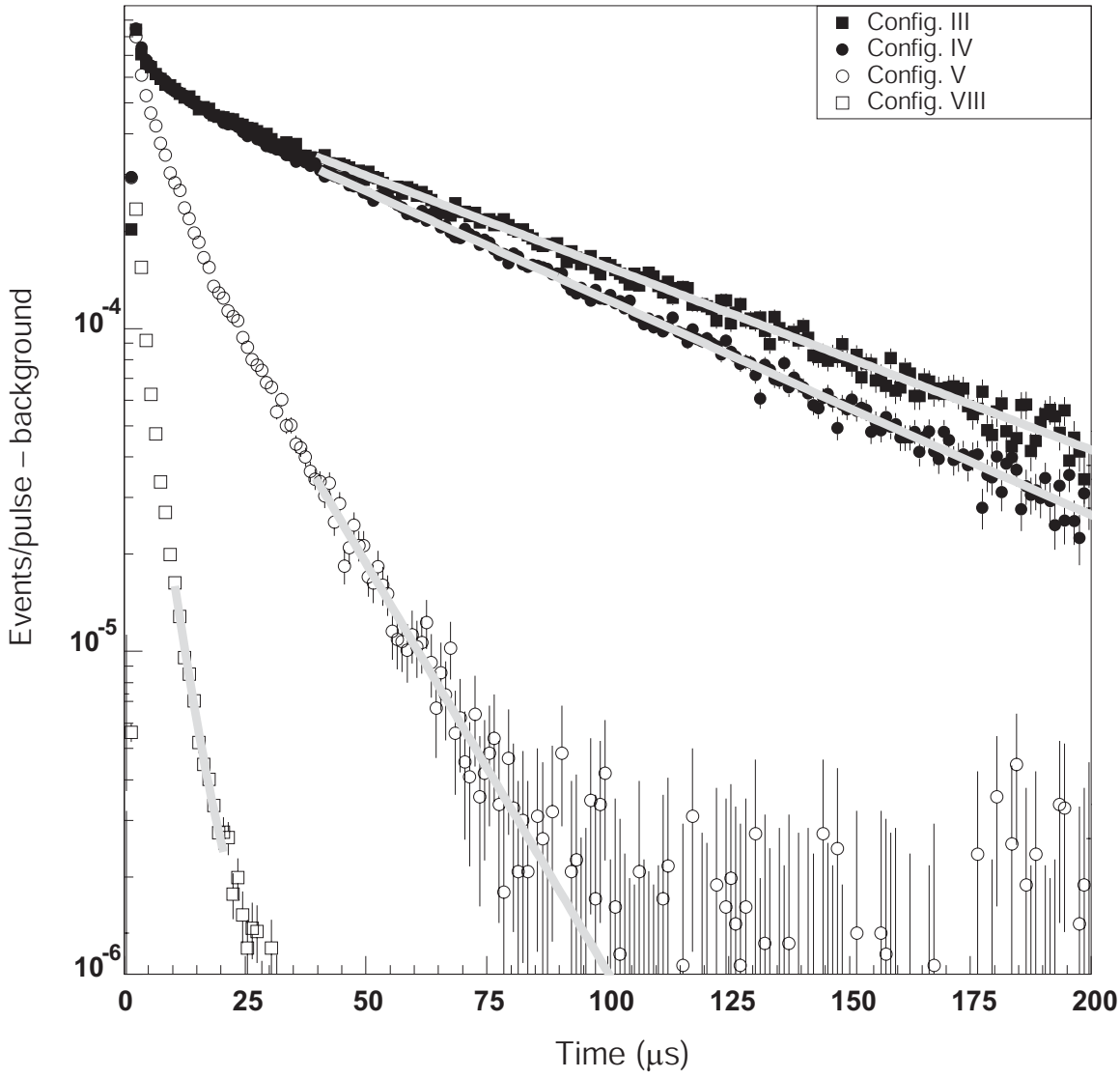

Fig. 7. Prompt response of MASURCA after a 1μs neutron burst, observed by the detector D5 placed in the core region (L5) for the different reactivity levels obtained in the configurations III, IV, V and VIII.

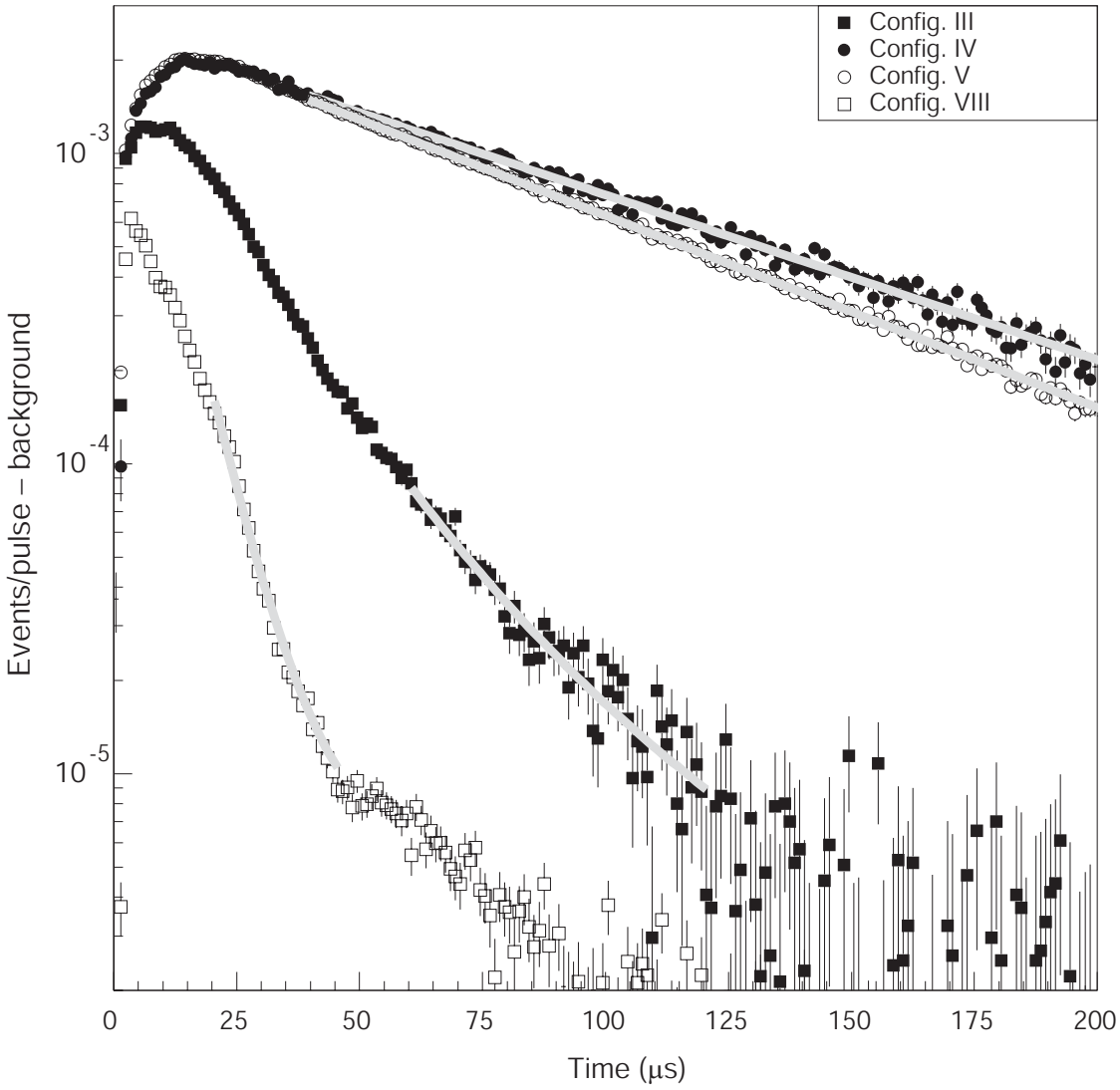

Fig. 8. Prompt response of MASURCA after a 1μs neutron burst, observed by the detector D1 placed in the reflector region (L1) for the different reactivity levels obtained in the configurations III, IV, V and VIII .

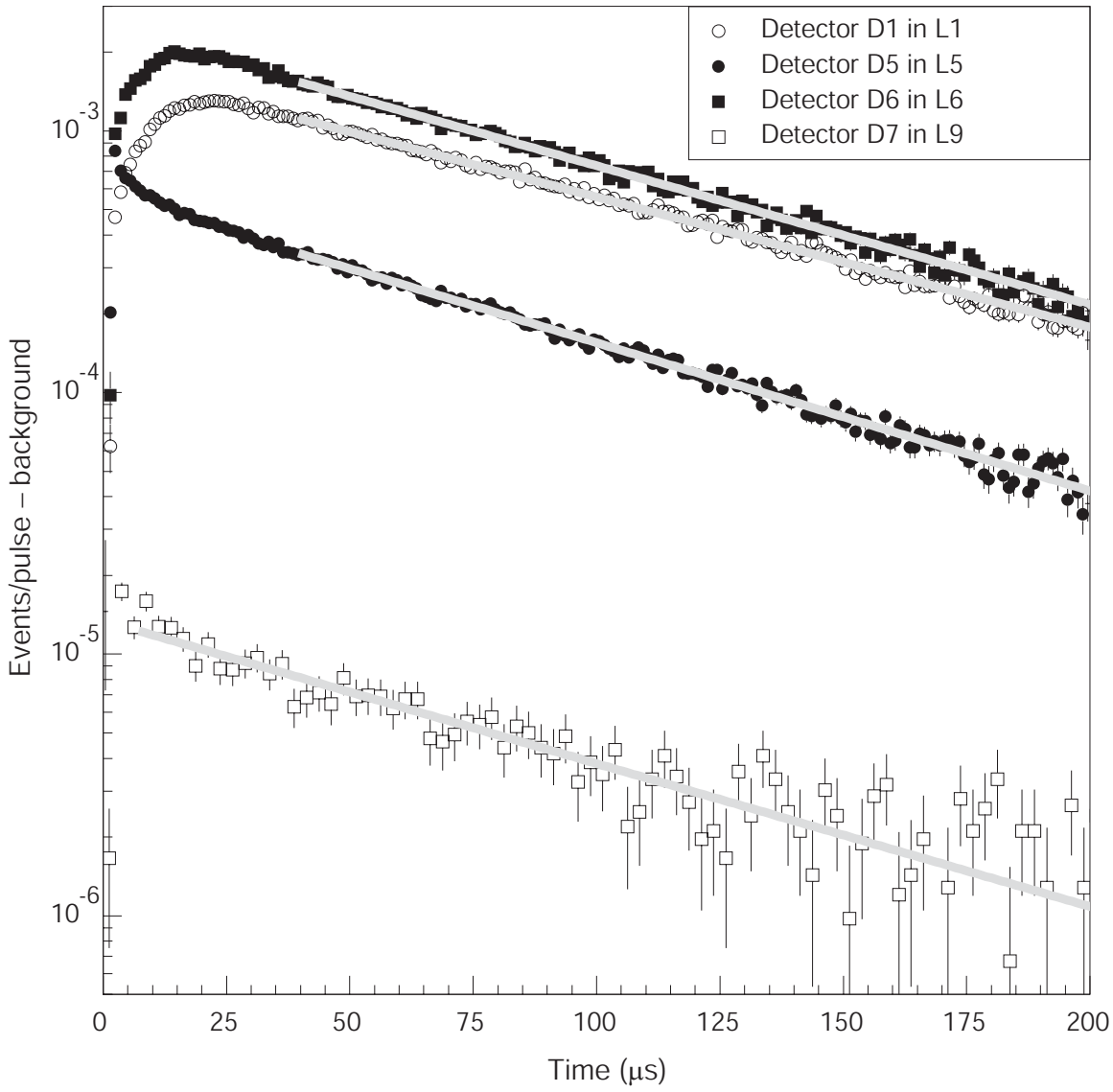

Fig. 9. Prompt response of MASURCA after a 1μs neutron burst for a same criticality level (configuration III) in different positions of the MASURCA reactor. Locations L5= core; L1 and L9 = reflector; L6=shield.

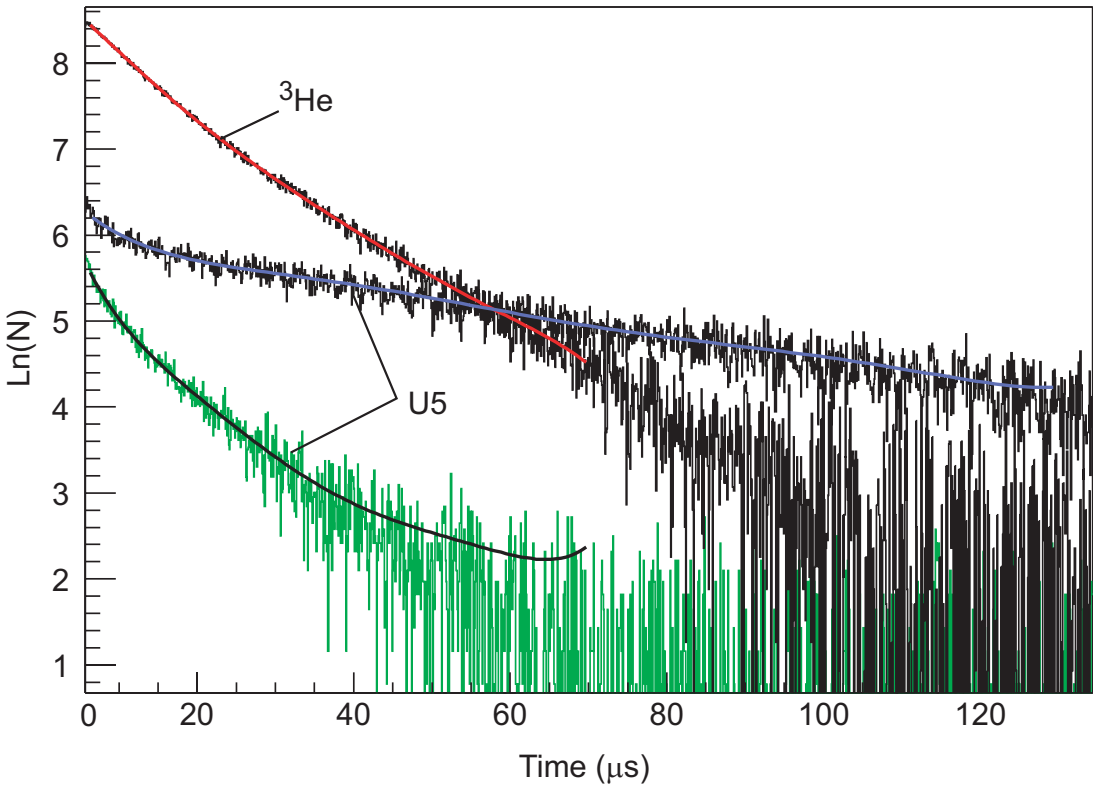

Fig. 10. Ln(N) time spectra obtained with a U5 FC (D12 in L12 for config. III and in L10 for config. V) and a ^{3}He detector (D13 in L13) in the fuel zone of MASURCA for two subcriticality levels $k_{e\ ff}$ = 0.995 and k_{eff} = 0.958 (configurations III and V). Plain curves are polynomial fits to the logarithm of the spectra.

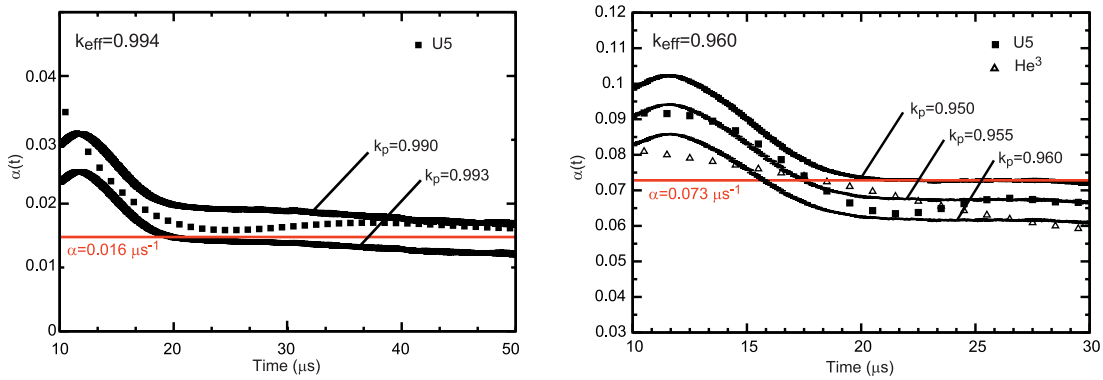

Fig. 11. Logarithmic derivatives of the fits of the experimental time spectra compared to several $\alpha_{kp}(t)$ calculated by the proposed method.

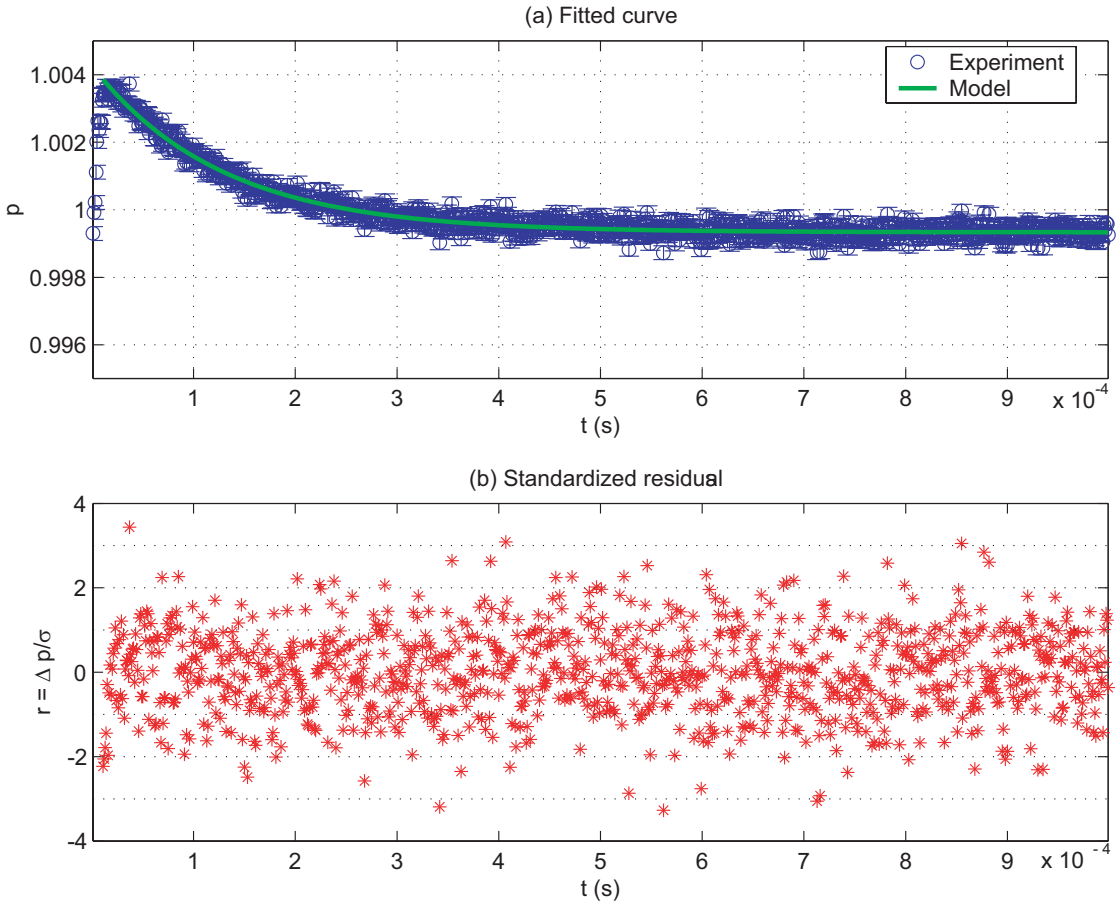

Fig. 12. Fit of the autocorrelation Rossi distribution.

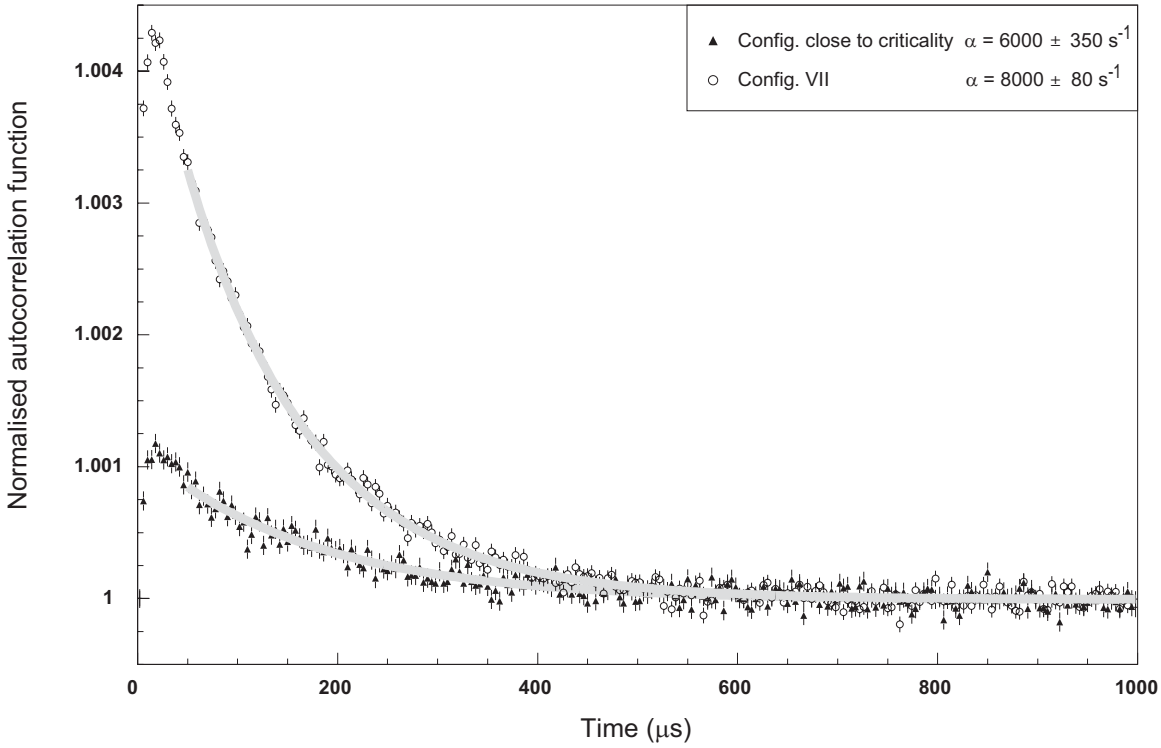

Fig. 13. Rossi distribution for two configurations.

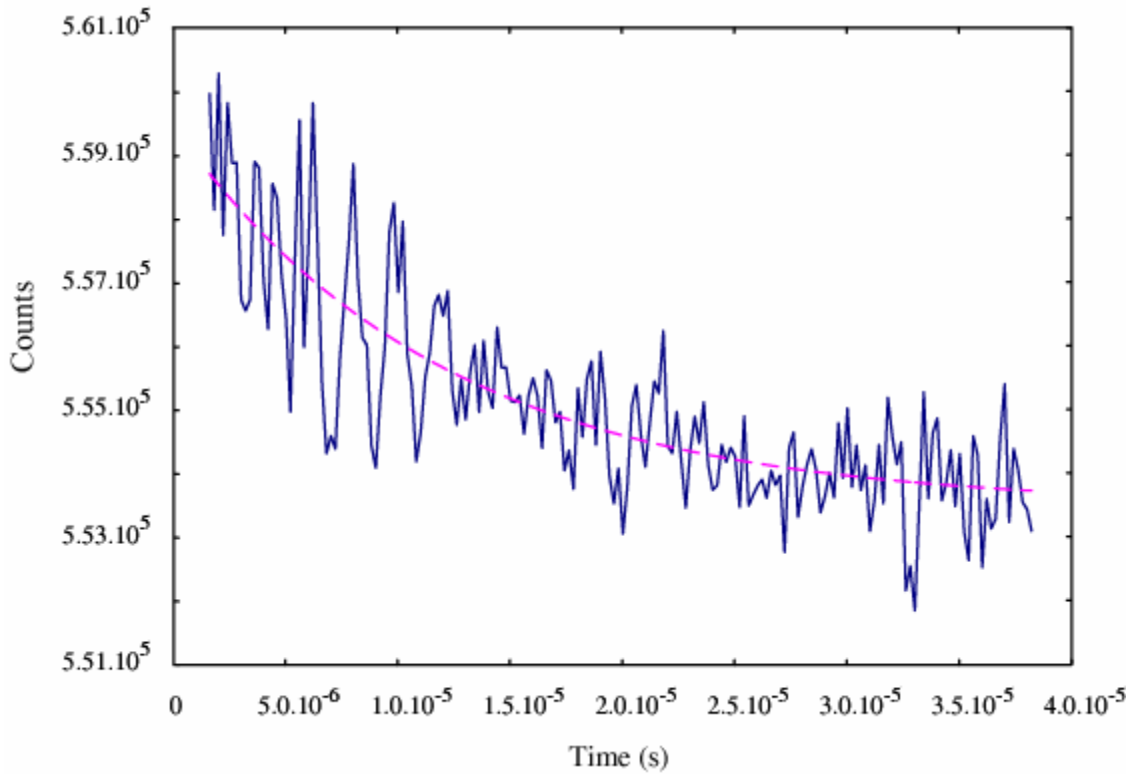

Fig. 14. Rossi-α distribution for a subcriticality level of -3795 pcm (configuration VI).

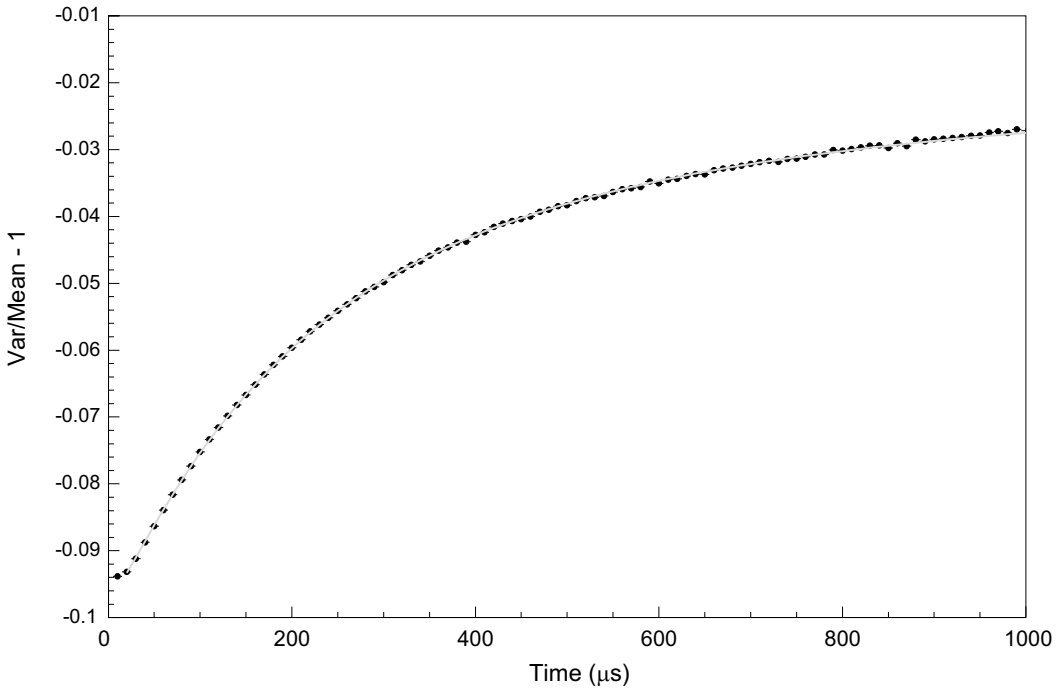

Fig. 15. Feynman-α distribution for a configuration close to criticality situation. The detector used is the same than in the Rossi-α case (configuration VII).

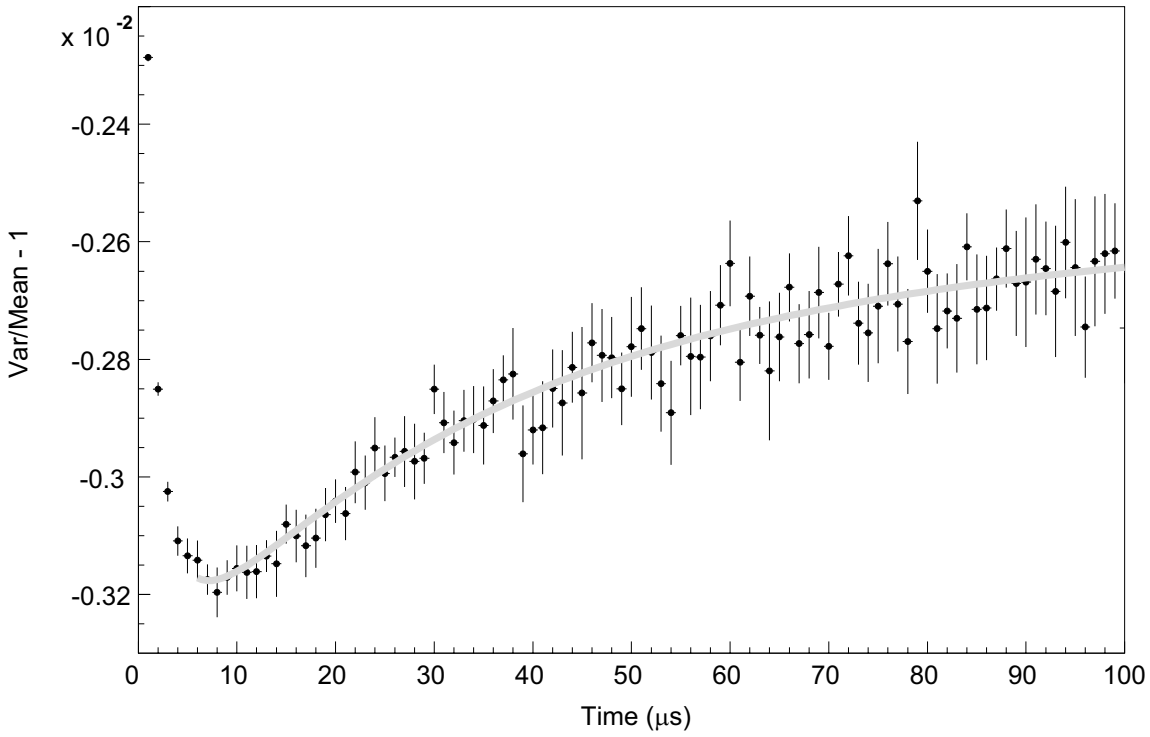

Fig. 16. Feynman-α distribution for a subcritical configuration. The detector used is the same than in the Rossi-α case (configuration VI).

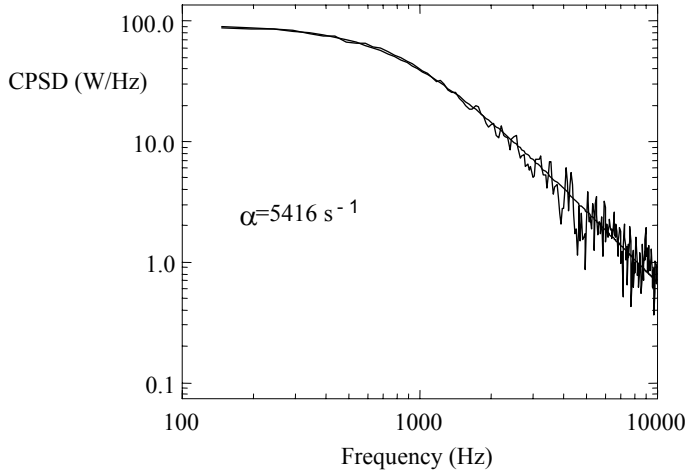

Fig. 17. The CPSD measured in continuous current mode with high-efficiency detectors at position L1 and L2. The α value from the fit equals about 5416 s^{-1}.

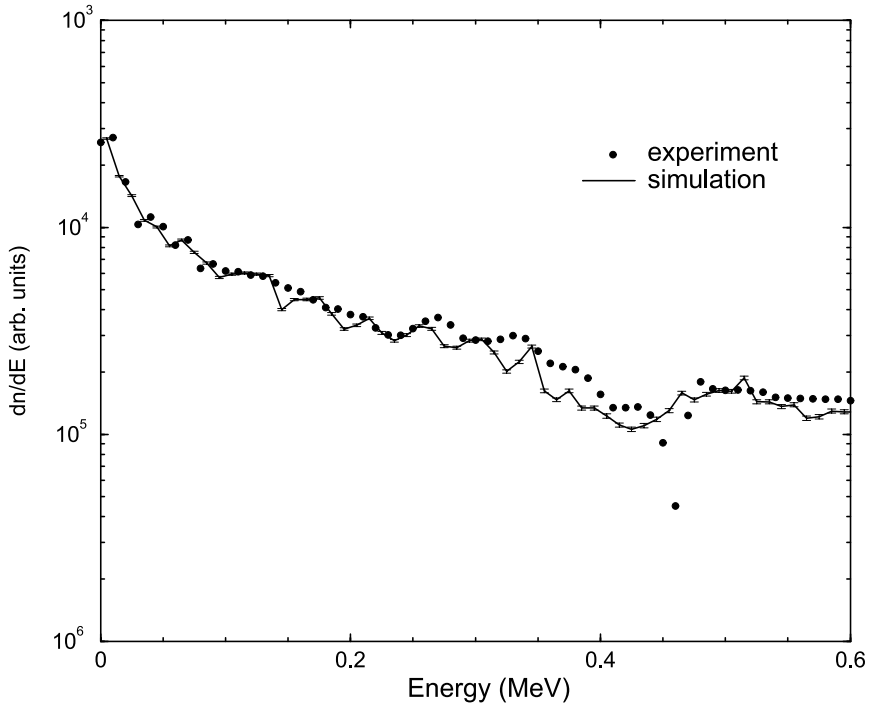

Fig. 18. Neutron spectrum in the fuel zone simulated with MCNP for k_{eff} = 0.96 (configuration V) compared to the spectrum measured with a ^{3}He counter.

TABLE I

Deuteron beam characteristics.

Beam energy (keV)	140 to 240
Peak current (mA)	50
Repetition rate (Hz)	10 to 5 000
Minimum pulse duration (10^{-9} s)	700
Mean beam current (μA)	200 (for a duty cycle of 5 000 Hz)
Spot size (mm)	≈ 20 in the diameter
Pulses reproducibility	Fluctuations at 1% level

TABLE II

Core configurations of measurements.

Configuration Name	Core loading and rod status	ρ (pcm)
I	Ref. 1114 cells 3SR up, SR1 down PR down	
II	Ref. 1114 cells 3SR up, SR2 down PR down	
III	SC0 1086 cells 4SR up PR up	SM: 452±30 PNS : 466±70
IV	SC0 1086 cells 4SR up PR down	SM : 593±40 PNS : 603±101
V	SC0 1086 cells 3SR up, SR1 down PR down	MSM : 4221±268
VI	Ref. 1115 cells 3SR up, SR2 down PR down	MSM: 3795±241
VII	Ref. 1115 cells 4SR up PR down	RD: 120±7
VIII	Ref.1114 cells 4SR down PR down	15000

TABLE III

Detector description.

Detector	**D1**	**D2**	**D3**	**D4**	**D5**	**D6**	**D7**	**D8**	**D9**	**D10**	**D11**	**D12**	**D13**
Isotope	^{235}U	^{235}U	^{235}U	^{235}U	^{235}U	^{235}U	^{237}Np	^{235}U	^{235}U	^{235}U	^{235}U	^{235}U	^{3}He
Mass (mg)	13	13	13	13	14.9	1070	2	14.9	1070	1110	1110	1000	gas counter

TABLE IV

Measurement locations.

Location	**L1**	**L2**	**L3**	**L4**	**L5**	**L6**	**L7**	**L8**	**L9**	**L10**	**L11**	**L12**	**L13**
X (cm)	50	-50	-50	50	10	70	-20	-80	10	-21.8	-0.6	-20	10
Y (cm)	45	45	-35	-35	-35	75	25	75	5	-25.6	-4.7	5	-45
Z (cm)	0	0	0	0	0	0	0	0	50	Z	Z	0	0

TABLE V

Locations of the activation foils used with the Reference MUSE-4 configuration.

Foil locations	**F1**	**F2**	**F3**	**F4**	**F5**	**F6**	**F7**	**F8**	**F9**	**F10**
X (cm)	21.2	-0.6	-7.4	-7.4	-7.4	-7.4	-53.0	-31.8	-10.6	0.0
Y (cm)	2.1	-4.7	-10.6	10.6	-21.2	37.1	2.1	2.1	2.1	2.1
Z (cm)	-9.5	-0.6	-0.6	-0.6	-0.6	-0.6	-9.5	-9.5	-9.5	-9.5

TABLE VI

C/E values for the spatial variation of different reaction rates.

Reaction	Threshold (MeV)	Code/Library	F2/F1 (C/E)	F3/F1 (C/E)	F4/F1 (C/E)	F5/F1 (C/E)	F6/F1 (C/E)
In115(n,γ)	/	**MCNP/JEF-2.2**	0.92 ± 0.07	0.94 ± 0.07	0.90 ± 0.07	0.94 ± 0.07	0.86 ± 0.07
Zn64(n,γ)	/	**MCNP/JEF-2.2**	0.96 ± 0.03	1.01 ± 0.03	1.01 ± 0.03	1.01 ± 0.03	0.97 ± 0.03
Au197(n,γ)	/	**MCNP/JEF-2.2**	0.98 ± 0.03	1.01 ± 0.03	0.96 ± 0.03	0.98 ± 0.03	1.00 ± 0.03
In115(n,n')	**1.2**	**MCNP/B6-dosi**	0.89 ± 0.02	0.95 ± 0.02	1.01 ± 0.02	1.02 ± 0.02	0.96 ± 0.02
Co59(n,p)	**2**	**MCNP/B6-dosi**	0.60 ± 0.06	0.84 ± 0.06	0.88 ± 0.06	1.01 ± 0.06	1.02 ± 0.06
Ni58(n,p)	**2.8**	**MCNP/B6-dosi**	0.84 ± 0.03	0.94 ± 0.03	1.02 ± 0.03	1.06 ± 0.03	0.99 ± 0.03
Zn64(n,p)	**2.8**	**MCNP/B6-dosi**	0.83 ± 0.05	0.96 ± 0.05	1.06 ± 0.05	1.08 ± 0.05	1.04 ± 0.05
Fe54(n,p)	**3.1**	**MCNP/B6-dosi**	0.82 ± 0.04	0.93 ± 0.04	1.00 ± 0.04	1.07 ± 0.04	1.00 ± 0.04
Fe56(n,p)	**6**	**MCNP/B6-dosi**	0.39 ± 0.06	0.75 ± 0.06	0.84 ± 0.06	1.00 ± 0.06	0.95 ± 0.06

TABLE VII

Calculated and measured spatial variations of spectral indices.

Spectral index [Threshold in MeV]	Type of result	F2/F1	F3/F1	F4/F1	F5/F1	F6/F1
Zn64(n,γ)/In115(n,n')	**Experimental**	1.60 ± 0.05	1.28 ± 0.04	1.28 ± 0.04	1.14 ± 0.04	1.10 ± 0.04
[-]/[1.2]	**MCNP/B6-dosi**	1.81 ± 0.09	1.40 ± 0.07	1.27 ± 0.06	1.15 ± 0.06	1.13 ± 0.06
Ni58(n,p)/In115(n,n')	**Experimental**	0.70 ± 0.03	0.84 ± 0.03	0.85 ± 0.03	0.90 ± 0.04	0.95 ± 0.04
[2.8]/[1.2]	**MCNP/B6-dosi**	0.65 ± 0.03	0.83 ± 0.04	0.85 ± 0.04	0.94 ± 0.05	0.98 ± 0.05
Zn64(n,p)/In115(n,n')	**Experimental**	0.65 ± 0.04	0.81 ± 0.04	0.80 ± 0.04	0.89 ± 0.05	0.90 ± 0.05
[2.8]/[1.2]	**MCNP/B6-dosi**	0.64 ± 0.03	0.82 ± 0.04	0.85 ± 0.04	0.95 ± 0.05	0.97 ± 0.05
Fe54(n,p)/In115(n,n')	**Experimental**	0.66 ± 0.03	0.83 ± 0.03	0.86 ± 0.03	0.90 ± 0.04	0.93 ± 0.04
[3.1]/[1.2]	**MCNP/B6-dosi**	0.64 ± 0.03	0.82 ± 0.04	0.86 ± 0.04	0.94 ± 0.05	0.98 ± 0.05

TABLE VIII

The reactivity worth measured and analyzed with inverse-point kinetics, compared with 2-D diffusion (FX2) and 3-D Monte-Carlo calculations (MCNP). The statistical errors in the Monte Carlo calculations are less than 50 pcm, giving an error for the rod worth of 74 pcm.

Config.	Run 1 $\widetilde{\rho}(pcm)$	Run 2 $\widetilde{\rho}(pcm)$	FX2 JEF-2.2	MCNP JEF-2.2	MCNP ENDF-B/VI Pb ENDF-B/V	MCNP ENDF-B/VI
I	D1: 3551 D2: 3886 D3: 3752 D4: 3384	D1: 3585 D2: 3685 D3: 3752 D4: 3216	3719	3652	3585	3685
II	D1: 4054 D2: 3350 D3: 4389 D4: 5025	D1: 4154 D2: 3317 D3: 4221 D4: 4925	4791	4556	4322	4489

TABLE IX

The reactivity worth measured and analyzed with inverse-point kinetics and corrected for the change of the spatial shape function, compared with diffusion calculations (FX2) and Monte-Carlo calculations (MCNP). Only the measured values differ from Table VIII. The statistical errors in the Monte Carlo calculations are less than 50 pcm, giving an error for the rod worth of 74 pcm.

Config.	Run 1 $\tilde{\rho}(pcm)$	Run 2 $\tilde{\rho}(pcm)$	FX2 JEF-2.2	MCNP JEF-2.2	MCNP ENDF-B/VI
I	D1: 3886 D2: 3116 D3: 3920 D4: 3987	D1: 3953 D2: 2982 D3: 3886 D4: 3819	3719	3652	3685
Average	$3909 \pm 201^{*}$			3618	
II	D1: 4590 D2: 4020 D3: 4690 D4: 4422	D1: 4657 D2: 3953 D3: 4489 D4: 4355	4791	4556	4489
Average	$4534 \pm 268^{*}$			4523	

*Averaged over the results of detectors D1, D3, and D4. Results of detector D2 have been discarded.

TABLE X

Values of α decay constant determination from different detector positions and GENEPI operation frequencies. σ_α refers to the uncertainty on α from the fitting procedure and δ describes the uncertainties produced by the selection of the fitting time interval.

Frequency (kHz)	α (s^{-1}) and σ_α/δ (%)							
	Core				Reflector			
	D5 in L5		D9 in L7		D1 in L1		D3 in L3	
1	12849	1.6/2.8	12645	1.4/3.7	12397	0.6/1.1	12336	0.6/1.0
2	13123	1.3/1.3	13014	1.0/2.6	12217	0.7/1.4	12314	0.7/1.7
3	13193	1.4/3.4	13484	1.1/2.0	12239	0.7/1.1	12225	0.7/1.5
4	13348	1.5/1.7	13213	1.2/3.0	12123	0.9/1.7	12292	0.8/1.2
$\bar{\alpha}/\sigma_{\bar{\alpha}}$	13128	1.6%	13089	2.7%	12244	0.9%	12292	0.4%

TABLE XI

Values of α decay constant determination from different detector positions and at different core configurations. δ describes the uncertainties produced by the selection of the fitting time interval, always larger than the fitting uncertainties.

	α and δ (s^{-1})		
Configuration	III	IV	V
Detector D5 in L5 (core)	13030 ± 240 s^{-1}	15600 ± 190 s^{-1}	62600 ± 3000 s^{-1}
Detector D3 in L3 (reflector)	12200 ± 150 s^{-1}	14300 ± 400 s^{-1}	60000 ± 4000 s^{-1}
Detector D8 in L8 (shield)	11500 ± 400 s^{-1}	13000 ± 400 s^{-1}	65000 ± 4000 s^{-1}
Detector D7 in L9 (reflector)	12600 ± 1000 s^{-1}	15600 ± 1000 s^{-1}	

TABLE XII

Values of ρ determination from different detector positions and for different core configurations using $\beta/\Lambda=5800s^{-1}$.

	ρ and systematic fit uncertainty (%)		
Configuration	III ρ_{SM}=-452±30pcm	IV ρ_{SM}=-593±40pcm	V ρ_{MSM}=-4221±268pcm
Detector D5 in L5 (core)	418 ± 14 pcm	566 ± 11 pcm	3280 ± 170 pcm
Detector D3 in L3 (reflector)	370 ± 9 pcm	491 ± 23 pcm	3130 ± 230 pcm
Detector D8 in L8 (shield)	329 ± 23 pcm	416 ± 23 pcm	3420 ± 230 pcm
Detector D7 in L9 (reflector)	390 ± 60 pcm	570 ± 60 pcm	

TABLE XIII

Reactivity computed from PNS experiments at different MASURCA configurations.

Config.	Type of experiment		ρ ($)	ρ (pcm)
III	Rod drop/SM		1.35 ±0.09	452±30
	Different Frequency method	Detector D5 in L5 core (1kHz – 2kHz)	1.28 ±0.05	429±17
		Detector D3 in L3 reflector (1kHz – 2kHz)	1.59 ±0.05	533±17
		(1kHz – 3kHz)	1.439 ±0.012	479±4
		(2kHz – 3kHz)	1.29 ± 0.03	432±10
V	Rod drop/MSM		12.6 ± 0.8	4221±268
	Diff. Freq. method	Detector D5 in L5 core (1kHz – 3.3kHz)	9.4 ± 1.0	3149±335
		Detector D1 in L1 reflector (1kHz – 3.3kHz)	10.4 ± 0.6	3484±201
III	PNS		1.39 ±0.21	466±70
	Inherent Source calibr. (1kHz)	Detector D1 in L1 reflector	1.591 ±0.021	533±7
		Detector D3 in L3 reflector	1.603 ±0.018	537±6
		Detector D9 in L7 core	1.60 ±0.60	536±20
		Detector D8 in L8 shield	1.69 ±0.10	566±34
IV	PNS		1.80 ±0.30	603±101
	Inherent Source calibr. (1kHz)	Detector D1 in L1 reflector	1.94 ±0.03	650±10
		Detector D3 in L3 reflector	2.01 ±0.03	673±10
		Detector D9 in L7 core	2.12 ±0.11	710±37
		Detector D8 in L8 shield	2.12 ±0.16	710±54
III	Rod drop/MSM		1.35 ± 0.09	452±30
	Inherent Source calibr. (1kHz)	Detector D9 in L7 core	1.28 ± 0.04	429±13
		Detector D9 in L7 core	1.30 ± 0.04	436±13

TABLE XIV

Fit results for the Rossi-α method.

Region	Detectors	$\alpha(s^{-1})$	$\sigma_\alpha(\%)$	r^2	RMSE
Reflector	(D10,D10)	8901	1.1	0.9725	1.0348
	(D11,D11)	7853	1.4	0.9591	1.0096
	(D10,D11)	7555	1.2	0.9670	0.9892
	(D11,D10)	7757	1.2	0.9662	1.0107
	(D3,D4)	7781	11.2	0.2636	1.0194

TABLE XV

Decay time obtained with Rossi-α technique with an inherent source.

Configuration	Detector	Approximate Reactivity level (pcm)	Time (s)	α (s^{-1})	α $\frac{E-C}{C}$
VII	D11 in L2	120	3057	8278	7%
	D11 in L2	120	6347	8403	6%
	D10 in L1	120	3604	9099	-2%
	D10 in L1	120	4124	9066	-2%
	D10 in L1	120	5692	9158	-3%
VI	D1 in L1 + D2 in L2	3795	8105	84034	-5%

TABLE XVI

Fit results for the Feynman-α method (configuration VII).

Region	Detectors	α (s^{-1})	σ_α (%)	r^2	*RMSE*
Reflector	(D10,D10)	8046	0.5	0.9997	1.62
	(D11,D11)	7691	0.5	0.9997	1.26
	(D10,D11)	7850	0.2	0.9999	0.46
Reflector	(D3,D3)	8917	2.6	0.9882	0.82
	(D4,D4)	9066	1.6	0.9955	0.54
	(D3,D4)	7891	1.9	0.9976	0.36
Core	(D8,D8)	9847	5.9	0.9314	0.82
	(D5,D5)	8359	7.1	0.9090	0.54
	(D8,D5)	7045	11.1	0.9243	0.36